



HAL
open science

A comparative study of the thermo-mechanical properties of polylactide/cellulose nanocrystal nanocomposites obtained by two surface compatibilization strategies

Hajar Faraj, Cyrille Sollogoub, Alain Guinault, Matthieu Gervais, Julien Bras, Hanène Salmi-Mani, Philippe Roger, Manon Le Gars, Sandra Domenek

► To cite this version:

Hajar Faraj, Cyrille Sollogoub, Alain Guinault, Matthieu Gervais, Julien Bras, et al.. A comparative study of the thermo-mechanical properties of polylactide/cellulose nanocrystal nanocomposites obtained by two surface compatibilization strategies. *Materials Today Communications*, 2021, 29, pp.102907. 10.1016/j.mtcomm.2021.102907 . hal-03412635

HAL Id: hal-03412635

<https://agroparistech.hal.science/hal-03412635>

Submitted on 3 Nov 2021

HAL is a multi-disciplinary open access archive for the deposit and dissemination of scientific research documents, whether they are published or not. The documents may come from teaching and research institutions in France or abroad, or from public or private research centers.

L'archive ouverte pluridisciplinaire **HAL**, est destinée au dépôt et à la diffusion de documents scientifiques de niveau recherche, publiés ou non, émanant des établissements d'enseignement et de recherche français ou étrangers, des laboratoires publics ou privés.

A comparative study of the thermo-mechanical properties of polylactide/cellulose nanocrystal nanocomposites obtained by two surface compatibilization strategies

Hajar Faraj^{1,2}, Cyrille Sollogoub², Alain Guinault², Matthieu Gervais², Julien Bras³, Hanène Salmi-Mani⁴, Philippe Roger⁴, Manon Le Gars³, Sandra Domenek¹

¹Université Paris-Saclay, INRAE, AgroParisTech, UMR SayFood, 91300, Massy, France

²Laboratoire PIMM, Arts et Metiers Institute of Technology, CNRS, Cnam, Hesam Université, 151, Boulevard de l'Hôpital, F-75013 Paris Cedex, France

³Univ. Grenoble Alpes, CNRS, Grenoble INP, LGP2, F-38000 Grenoble, France

⁴Institut de Chimie Moléculaire et des Matériaux d'Orsay, Université Paris-Saclay, CNRS, 91405 Orsay, France

Corresponding author: Sandra Domenek, UMR SayFood (Université Paris-Saclay, INRAE, AgroParisTech), 1 rue des Olympiades, 91300 Massy, France; sandra.domenek@agroparistech.fr

Keywords: PLA, nanocellulose, surface compatibilization, mechanical properties, surface interaction, percolation

Abstract

Nanocomposites of poly(lactide) (PLA) and cellulose nanocrystal (CNC) were fabricated using two different types of covalently grafted surface compatibilizers, namely fatty acids (lauric or stearic acid) and poly(glycidyl methacrylate) (PGMA) bearing reactive epoxy end-groups. Temperature-Modulated DSC analysis informed on weak attractive interaction of PLA and CNC-g-lauric acid and weak plasticizing of CNC-g-stearic acid. Despite that a homogenous dispersion of up to 50 wt.% of CNC in PLA was obtained and the rubbery elastic moduli increased 150-fold as compared to PLA. CNC-g-PGMA phase-separated in PLA but partially to it at the interface. It yielded a 40-fold increase of rubbery plateau moduli. The data analysis with the Ouali model for percolated systems and the Halpin-Tsai model for composites with short fibres showed that CNC-g-lauric acid percolated in PLA. However the effective modulus

of the percolated network was smaller than that of unmodified CNC. Reactive compatibilization of PLA with CNC-g-PGMA prevented percolation but lead to high filler/matrix coupling. In that case, the modulus increase could be described using the Halpin-Tsai model. In conclusion, surface compatibilizing even if developing only weak interactions with the polymer matrix helps to obtain homogenous nanocomposites, but the strength of the percolated network is lowered because it weakens also the CNC/CNC interactions. Reactive surface compatibilizing using polymers can be an interesting alternative, but needs to be optimized to take advantage of the high filler/matrix coupling and avoid phase separation.

1. Introduction

Cellulose nanocrystals (CNC) are cellulosic nanoparticles that are very attractive nanofillers considering their renewability, abundance, biodegradability, and outstanding mechanical properties (modulus and strength). The geometrical dimensions of rod-like CNC depend strongly on the cellulose source, but typical values of length and aspect ratio are comprised between 100 to 1000 nm and 5 to 100, respectively [1, 2]. Obtained by acid hydrolysis of cellulose fibers, CNC have high crystallinity and high elastic modulus reported to be between 100 and 150 GPa [3-5]. They are highly polar because of numerous hydroxyl groups (-OH) on their surface which can reach concentrations of 7.2 groups/nm² in cellulose nanocrystals. This ensures good surface reactivity [6]. The formation of numerous hydrogen bonds can create a 3D rigid and tough percolated network. Favier et al. [7, 8] reported for the first time the outstanding reinforcing effect of the percolating network on mechanical properties. An improvement of more than 2 orders of magnitude in rubbery state was obtained at a concentration 6 wt.% in the thermoset polymer (poly(S-co-BuA)). The mechanical properties were described by the percolation model developed by Ouali [9].

CNC have been incorporated in many polymer matrices (thermosets or thermoplastics) in order to obtain nanocomposites with improved properties [10-12]. Among the different possible matrices, biobased and biodegradable polymers are of special interest because the resulting nanocomposite is fully biobased. Polylactide (PLA) is a promising commercially available polyester. Despite its numerous advantages, PLA suffers for some drawbacks, such as moderate stiffness and low heat deflexion temperature [13] and low elastic modulus in the rubbery state [14]. This limits its use in applications, where the service temperature exceeds its glass transition temperature, typically in packaging technologies using hot-filling or sterilization of foodstuff inside the package. To overcome this drawback, semicrystalline PLA can be used, but the crystallization kinetics of PLA are rather slow [15]. An alternative is the inclusion of charges

and, in particular of nanocharges. PLA/CNC nanocomposites were studied over the past few decades [16]. The most important challenge to reach high performance of PLA/CNC nanocomposites remains the dispersion of the CNC in the matrix. Due to the strong hydrogen bonds between the nanoparticles, CNC easily form almost irreversible aggregates once dried and are very difficult to disperse in non-polar polymer matrices such as PLA [4]. Taking advantage of the reactivity of the hydroxyl groups on the CNC surface, chemical surface modification is used to enhance the compatibility and dispersion in polymer matrices. Many such strategies have been proposed: esterification [17-20], acetylation [21, 22], grafting of polymer chains [20, 23-25], non-covalent surface modification [26-29].

However, as clearly pointed out by Miao & Hamad [10], uniform dispersion of CNC in the polymer matrix is not the unique condition to reach high mechanical performance. Additionally, the concentration of the nanocharge needs to be higher than the percolation threshold and the modulus of the percolating network should be high. The contribution of the interaction between polymer and CNC can only be neglected in case the modulus of the percolated network is much higher than that of the polymer matrix. Both, percolation threshold and modulus will be impacted by the surface grafting of CNC, though. Hydrophobic surface grafts hinder the creation of hydrogen bonds between individual CNC and can potentially decrease the strength of the percolated network and increase the percolation threshold. This phenomenon was shown on the example of rubber nanocomposites using chemically modified chitosan nanocrystals [30]. The result could be extended to CNC, but it is not clearly discussed yet. Indeed, collecting the data of more than 20 different studies, Vatansever et al. [16] showed that the actually observed improvements in the elastic moduli of PLA/CNC nanocomposites were generally modest. Best results were an increase of a factor 2 of the modulus in the glassy state [20] and around ten in the rubbery state [20, 31].

To investigate in more detail and report on the impact of the CNC surface modification on the mechanical strength of PLA/CNC nanocomposites, we build on recent results obtained by Le

Gars et al. [25, 32]. They developed a scalable CNC surface esterification method[32] based on the SolReact procedure proposed by Espino et al. [17, 33] using fatty acids (lauric acid C12 and stearic C18). Fatty acids are abundant and non-toxic molecules and were grafted using an in-situ solvent exchange mechanism at atmospheric pressure and relatively low temperature (110 °C). Furthermore, they presented a grafting-from method of growing poly(glycidyl methacrylate) (PGMA) from the CNC surface via surface-initiated atom transfer radical polymerization [25]. The specificity of this compatibilizer is that it bears reactive epoxy groups, which are potentially able to crosslink among each other and with PLA. Both compatibilizers were grafted to the same type of CNC, which allowed for direct the comparison of the mechanical performance PLA/CNC nanocomposites based on a very different compatibilizing mechanisms. To avoid interference in the interpretation caused by PLA crystallization, we used a grade with high D-lactic acid content, unable to crystallize under common processing conditions. Analysis of the relaxation properties of the nanocomposites and their elastic moduli was performed using Temperature-Modulated Differential Scanning Calorimetry (TM-DSC) and dynamic mechanical analysis (DMA). In the aim to evaluate the effect of CNC percolation on the viscoelastic moduli, samples with a wide CNC concentration range (up to 50 wt.%) were fabricated by solvent casting. The effects of CNC on the moduli were analyzed and quantified with the help of mechanical modelling.

2. Experimental section

2.1. Materials

Poly(lactic acid (PLA) INGENEO pellets “NatureWorks 4060D” were purchased from Resinex, France. This amorphous grade has a D-lactic acid content of 11 ± 1 mol % according to supplier’s specifications, which prevents crystallization under common laboratory conditions due to extremely slow crystallization kinetics. The cellulose nanocrystals powder (CNC) was

supplied by CelluForce (Canada). The cellulose nanocrystals were extracted from wood fibers and spray-dried by the supplier. Lauric acid ($\geq 98\%$) and stearic acid (Reagent grade 95%) were supplied by Sigma-Aldrich Chimie (France). Dichloromethane (CH_2Cl_2) was supplied from Carlo Erba reagents (France), and used without further purification (purity over 99.8 %).

2.2. Preparation of surface modified CNC

2.2.1. SI-ATRP of Glycidyl methacrylate on pre-functionalized CNC

CNC were modified by a surface-initiated ATRP polymerization (SI-ATRP) of glycidyl methacrylate (GMA), as described by Le Gars et al. (2020) [25]. Briefly, CNC were first modified with α -bromoisobutyryl bromide reagent (BIB), in order to introduce brominated initiator sites at their surface for further radical polymerization. Recovered CNC-Br were then subjected to several freeze-thaw cycles to remove oxygen, followed by the SI-ATRP of GMA for one hour involving GMA/EBIB/PMDETA/CuBr (ethyl α -bromoisobutyrate (EBIB)/N,N,N',N'',N'''-pentamethyldiethylenetriamine (PMDETA)/Copper (I) bromide (CuBr)) reagents system with 100:1:1:1 composition ratio. At the end of the reaction, polymerized CNC-PGMA-Br were extensively washed by successive centrifugation cycles (9000 rpm, 15 min, 5 °C) in dichloromethane to remove all unreacted reagents and homopolymer PGMA polymerized from EBIB as sacrificial initiator. CNC-PGMA-Br were stored in dichloromethane until further use and characterizations. Characterizations of surface polymerized CNC-PGMA-Br were carried out by Le Gars et al. (2020) [25]. In short, after having proved the efficiency of the polymerization of GMA from the surface of the CNC, the degree of substitution of surface-polymerized CNC was calculated equal to 0.2. Theoretical degree of polymerization of GMA was chosen equal to 100. After taking in consideration the conversion of 46 % after one hour of polymerization, the degree of polymerization of the PGMA on the surface of the CNC was close to 46, with a proportion of around 50 % in mass of polymer in the sample. By investigating the crystallinity of the CNC-PGMA-Br by XRD, the spectra showed signals of both the crystalline cellulose I β and amorphous PGMA.

Furthermore, dynamic light scattering analysis of CNC-PGMA-Br showed a mean diameter of the particles equal to 164 nm, highlighting the presence of nanosized particles.

2.2.2. Surface esterification of CNC with lauric and stearic acid

The CNC esterification [32] procedure was adapted from the SolReact protocol [17] for non-water soluble organic acids. The aqueous CNC suspension was solvent exchanged to acetone by successive centrifugation cycles (10000 rpm, 5 °C, 15 min) in water, ethanol, and then acetone. The acetone suspension (1 wt.%) was then introduced in a flask mounted with a distillation system, and heated at 110 °C. A catalytic amount of sulfuric acid H₂SO₄, as well as a large excess of lauric or stearic acid (weight ratio CNC: acid = 1: 100) were added to the reaction media. After total acetone evaporation, CNC were dispersed in melted lauric or stearic acid, which thus acted as the reaction solvent, and the system was let under stirring for 8 h. At the end of the reaction, CNC were extensively washed with ethanol by successive centrifugation cycles (10000 rpm, 25 °C, 15 min). The recovered modified CNC-g-lauric acid or CNC-g-stearic acid in ethanol were then stored in a hermetically closed container until further use. The chemical characterization of the surface grafted CNC was reported in Le Gars et al. (2020) [32]. The determined by XPS and solid-state ¹³C NMR the degree of surface substitution to equal to 0.14 for lauric acid and 0.35 for stearic acid. The surface esterification increased the of the water contact angle to 80° ± 2 for lauric and 82° ± 4 for the stearic acid. The crystallinity index was calculated from XRD analysis using the Segal height peak method [34] and was equal to 83 % for both acids, and the nanosized structure was confirmed by TEM analysis.

2.3. Nanocomposite preparation

PLA pellets and CNC powder were stored in a closed desiccator at room temperature containing silica gel. Additionally, the CNC powder was vacuum-dried for 2 days at 80 °C prior to solution preparation. The moisture content after drying was approximately 4 wt.% as determined by thermogravimetric analysis.

A solution of 10 wt.% PLA was prepared by dissolution of the pellets in CH₂Cl₂ at room temperature for 12 hours. Dry unmodified CNC were dispersed in CH₂Cl₂ and sonicated using an ultrasound homogenization (Vibra-Cell™ Ultrasonic liquid processor, Sonics & Materials, USA) (10 kJ/g of CNC) [35], while surface-modified CNC were solvent exchanged and suspended in CH₂Cl₂, followed by a sonication at the same energy. The suspension was kept in an ice bath to avoid solvent evaporation. The dispersion of CNC was controlled before used with the help of dynamic light scattering (DLS) instruments (Malvern Instruments, UK) to ensure the nanometric character of the solution. PLA solution and CNC suspension were mixed using a homogenizer (Ultra-Turrax, IKA) for approximately 5 min. The sonication was performed to ensure the complete homogenization and to extract any air bubbles from the mixture. The final mixture was then cast into Teflon Petri dishes and left under the laboratory hood at room temperature for 48 h. The films were removed from the Petri dishes and put in a vacuum oven at 60 °C for 24 h for further drying. PLA/CNC mixtures, PLA/CNC-g-stearic acid or lauric acid containing 0, 5, 10, 30 and 50 wt.% of cellulose nanocrystals were prepared. The CNC percentage is based on the total weight of dried materials (PLA/CNC), after solvent evaporation. Since the proportion of the grafted polymer (PGMA) was estimated to 50 wt.%, the used modified-CNC weight was based on the CNC weight-fraction alone, i.e., for 1 mg of CNC, 2 mg of CNC-g-PGMA were used in the fabrication of nanocomposites.

A hot press (Gibitre Instruments, Italy) was used to prepare the final nanocomposites. The films obtained from solvent casting were sandwiched between two Teflon sheets in a 100 µm mold. The set up was then pressed at 180 °C and 150 bar for 3 min. After pressing, the samples were cooled down to room temperature. The compressed PLA/CNC samples were denominated as PLA/X%CNC, where X represents concentration of CNC, e.g. PLA/10% CNC indicated a film containing 90 wt.% PLA and 10 wt.% CNC.

2.4. Nanocomposite characterization

2.4.1. Scanning Electron Microscopy (SEM)

The morphology evaluation of the cross-sections obtained by cryo-fracture was studied using an EVO MA10 SEM from Zeiss with a tungsten electrode, under an acceleration voltage of 15 kV. Specimens were sputtered with a thin layer of gold. Image acquisition was performed using SmartSEM User Interface software. All measurements from the images were recorded and analyzed using the software ImageJ.

2.4.2. *Transmission Electron Microscopy (TEM)*

UltraThin PLA/CNC film sections (≈ 70 nm) were obtained by using a microtome (Leica EM UC6) equipped with a DiATOME Diamond knife. The obtained sections were placed on TEM Copper grids coated with amorphous carbon, after brief plasma treatment (glow discharge). TEM images acquisition was performed on CERMAV's Microscopy platform (NanoBio-IMCG, Grenoble, France), by the means of the Transmission Electron Microscope FEI/Philips CM200. The used acceleration voltage was 200 kV and the images were recorded thanks to a TVIPS TemCam F216 digital camera.

2.4.3. *Dynamic Light Scattering (DLS)*

Dynamic light scattering measurements were performed using a MasterSizer 2000 (Malvern Instruments, UK). Suspensions of modified and unmodified CNC were prepared and set at 10^{-2} wt.% concentration in the used dispersant. The size distribution of nanocellulose particles was measured in different solvents as dispersants: water, ethanol, acetone, and CH_2Cl_2 (with a respectively refractive index of 1.333, 1.361, 1.36, and 1.424 at 25.0 °C).

2.4.4. *Modulated Temperature Differential Scanning Calorimetry (TM-DSC)*

Thermal characterization was performed using temperature modulated differential scanning calorimeter (TM-DSC Q100) from TA Instruments (France). The N_2 flow was 50 mL min^{-1} . The apparatus was calibrated in temperature and energy using Indium. The specific heat capacity (C_p) for each sample was calibrated using a sapphire reference. The modulation mode was heat-only with an oscillation amplitude of $0.318 \text{ }^\circ\text{C}$, a period of 60 s and a heating rate of $2 \text{ }^\circ\text{C min}^{-1}$. The samples ($3 \pm 1 \text{ mg}$) were placed in TZero aluminum pans. Before the

measurements, the dried films were stored in a desiccator at room temperature for at least one week over silica gel. The measurements were duplicated to ensure repeatability.

2.4.5. *Thermogravimetric Analysis (TGA)*

Thermal degradation of PLA, CNC and PLA/CNC nanocomposites was determined by thermogravimetric analysis using a TGA Q500 from TA Instruments. This instrument was weight-calibrated with standards of 100 mg and 1 g. A temperature calibration was performed at room temperature, using the Curie temperature of Nickel. Scanning conditions were set from room temperature to 350 °C, using the High-Resolution (Hi-Res) mode with standard settings. This method allows to separate closely occurring events and transitions thanks to a dynamic heating rate. The equipment automatically reduces the heating rate near zero, when it detects a weight change and accelerates again when the weight change is over. The evaporation of molecules with one characteristic temperature happens therefore in nearly isothermal mode. The used samples had a mass of 10 ± 2 mg and were tested under N₂ flow. The determination of modified CNC concentration in the dichloromethane solution after the solvent exchange was determined by thermogravimetric analysis using a TGA Q500 from TA Instruments. Scanning conditions were set from room temperature to 150 °C, using a Hi-Res mode, under N₂ flow. The samples were sealed in DSC capsules with a perforated lid and frozen using liquid nitrogen before placed on the sample holder platform to avoid premature solvent evaporation. All measurements were duplicated.

2.4.6. *Dynamic Mechanical Analysis (DMA)*

Thermomechanical properties of the samples were measured thanks to a DMA Q800 (TA Instruments, France). The samples were conditioned in a desiccator at room temperature and rejuvenated at 70 °C for 30 min prior to the tests. The dimensions of the tested samples varied between 90 and 190 μm thickness, 5 ± 0.5 mm width and 13 ± 2 mm length. The operation mode used was tensile at a frequency of 1 Hz, a heating ramp from 30 to 180 °C, using a heating rate of 3 °C min⁻¹. To guarantee that the mechanical response was within the linear viscoelastic

region, an amplitude sweep was carried out in the glassy (at 30 °C) and the rubbery state (at 65 °C) of PLA and the maximum strain amplitude of 0.1 % was selected.

3. Results and discussion

3.1. Thermo-degradation properties of PLA/CNC nanocomposites

Typical melt processing temperatures of PLA range between 150 and 180 °C [6], and our sample preparation method involved heat-treatment at 180 °C. Therefore, we tested the thermal stability of CNC and the nanocomposites by TGA. As displayed in **Figure 1**, neat CNC was thermally stable at the processing temperature. The powder exhibited a first weight drop of 4 wt.% from 30 to 110 °C, which corresponds to the water content. Thermal degradation of CNC started (**Figure 1a**) with an onset at 269 °C, due to the depolymerization of the polysaccharides by transglycosylation, followed by dehydration and scission of sugar units, generating a high amount of carbonized residues/char (ca. 35 wt. %) after evaporation of volatile compounds (glyoxal and acrolein for example) [36]. The degradation behavior of PLA (**Figure 1a**) was coherent with already reported values [37]. It consisted in a single degradation step with an onset of 312 °C and had its maximal degradation rate at $321 \pm 1^\circ\text{C}$ (**Figure 1c**). The thermal degradation of PLA/CNC-g-lauric acid composites containing 5 and 10 wt.% CNC-g-lauric acid had an onset of degradation at 305 °C, which is shifted by 7 °C to lower temperatures as compared to neat PLA (**Figure 1a**). At this concentration, the presence of the grafted CNC did not impact importantly the thermal stability of the PLA matrix. At higher CNC-g-lauric acid contents (30 and 50 wt.%), a two-step degradation was observed. For the sample containing 30 wt.% CNC-g-lauric acid, a first degradation appeared with a first maximum decomposition peak at 254 °C related to the CNC fraction, and a second maximum degradation peak at 322°C related to PLA. Similarly, the sample containing 50 wt.% CNC-g-lauric acid exhibited a first decomposition peak at 249 °C linked to the grafted CNC fraction and a second one at 324 °C.

Composites containing CNC-g-stearic acid showed two degradation steps. PLA/10%CNC-g-stearic acid showed a first weight loss at 298 °C, followed by a second one at 309 °C, while the sample containing 30 wt.% exhibited a first degradation peak at 282 °C then 318 °C. Similarly to the lauric acid-modified CNC nanocomposites, the first drop was associated to the grafted CNC fraction and the latter to the PLA fraction. The thermal stability of the grafted CNC is lower compared to neat CNC, most probably because of the lower degradation temperature of the fatty acids (see supplementary information). The degradation temperature was however still higher than 180 °C, the processing temperature. With the help of the degradation data, we calculated the effective weight percentage of grafted CNC, which amounted to the theoretical weight percentage \pm 3 wt.% (see supporting information for detailed table).

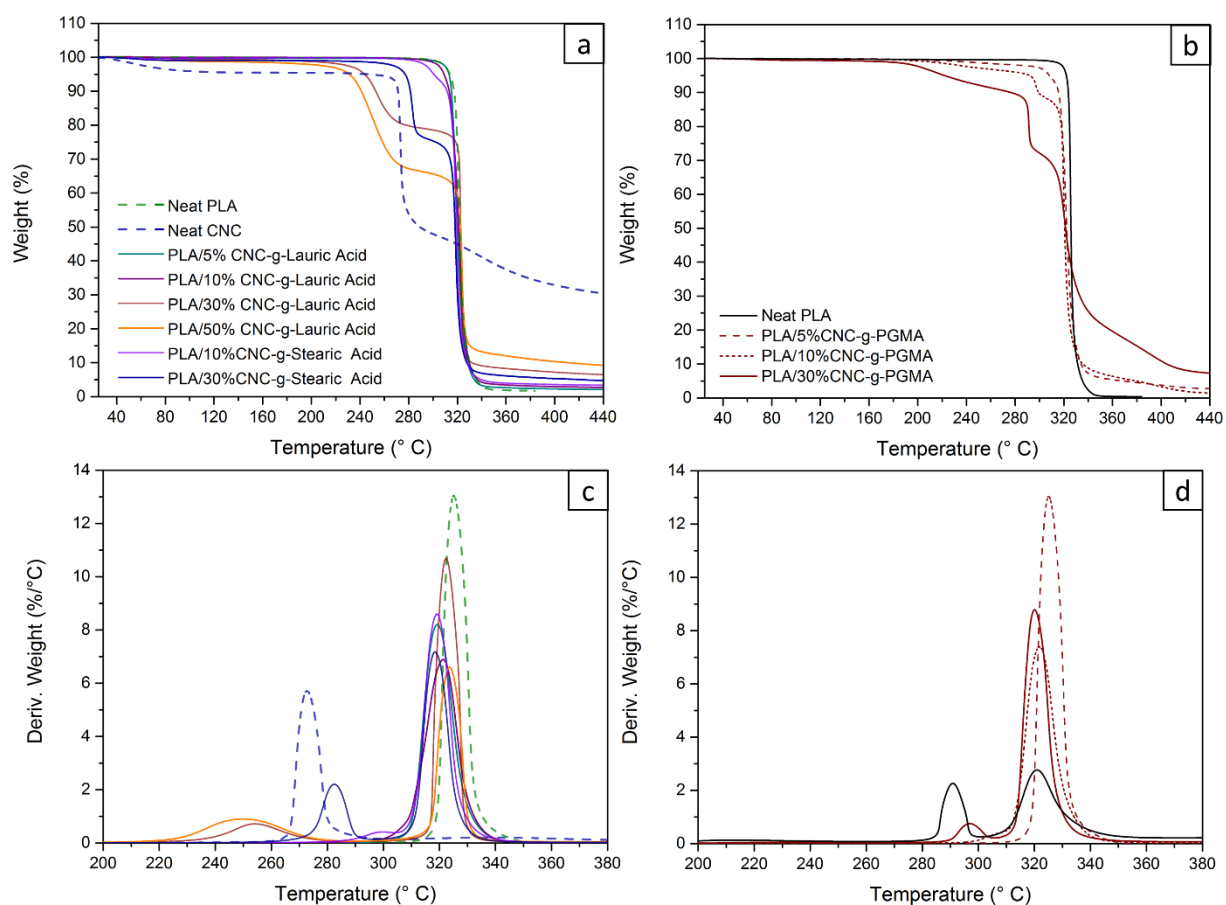


Figure 1. TGA and DTGA curves of PLA/CNC nanocomposites grafted with lauric or stearic acid (a, c) and PGMA (b, d).

Figure 1b shows the thermograms of PLA/CNC-g-PGMA nanocomposites. Similar to the previous results, at small concentrations, no impact on the degradation temperature of PLA was observed. The samples containing higher CNC contents exhibited degradations of at least two steps: a continuous weight loss from 220 °C to 300 °C, and from 190 °C to 295 °C, respectively for 10 and 30 wt. %, which can be associated to CNC-g-PGMA. In conclusion, TGA results showed that the included CNC at high percentage decreased the thermal stability of PLA, but the degradation onset temperatures were still higher than commonly used melt processing temperatures and the thermal treatment temperature of the sample preparation method.

3.2. Morphological analysis of CNC and nanocomposites

Figure 2a shows the estimation of the size of CNC and grafted CNC by DLS in aqueous suspension and acetone. DLS analysis overestimates the size of the modified CNC particles, because the shape factor of the cylindrical particles cannot be accounted for. Therefore, DLS was used only on a comparative basis between modified and unmodified CNCs. The quantification of the data is reported in **Table 1**. The commercial CNC can be efficiently dispersed in water and the size is consistent with literature data on CNC from wood and the commercial data sheet [35, 38]. The casting procedure for the fabrication of the nanocomposites needs a solvent exchange towards less polar media, because grafted CNC and PLA cannot be dispersed in water. For that purpose, the choice of the proper solvent, here acetone, was done using Hildebrand's solubility parameters as proposed by Bruel et al. (2018) [39]. Water has a high dispersion power for neat CNC because it can break efficiently hydrogen bonds and stabilize negatively charged CNC particles. After compatibilization, most hydroxyl groups are engaged in the ester bond with lauric or stearic acid, which decreased the dispersibility in water, but increased it in organic solvents. When native CNC is solvent exchanged to acetone, which

is still a quite polar organic solvent, the average size increased due to slight aggregation. Moreover, surface esterification of CNC increased the average size of CNC (**Table 1**).

Table 1. Morphological analysis of modified and unmodified CNC by DLS, TEM and SEM.

Samples	Degree of substitution (DS)	DLS		CNC length (nm)	TEM		Percolation threshold (Vol.%)	Percolation threshold (wt.%)
		Apparent CNC length (nm)	Polydispersity index		CNC diameter (nm)			
Hydrated CNC CelluForce	-	120	0.36	186 ± 42	8 ± 1	3.01 ± 35 %	3.85	
CNC CelluForce in acetone (solvent-exchanged)	-	307	0.14	-	-	-	-	
CNC-g-lauric acid in acetone	0.14 [32]	386	0.25	309 ± 69	29 ± 15	6.57 ± 74 %	8.4	
CNC-g-stearic acid in acetone	0.35 [32]	405	0.31	351 ± 73	31 ± 16	6.18 ± 71 %	7.9	
CNC-g-PGMA in CH ₂ Cl ₂	0.2 [25]	164		-	-	-	-	

For exacter analysis, TEM pictures of CNC and grafted CNC were taken (**Figure 2b-d**) and the quantification of the sizes is given in **Table 1**. **Figure 2b** shows a majority of isolated CNC particles with an average length of 186 nm and a diameter ranging from 6 to 10 nm. After esterification, the isolated particles maintained a similar length, and formed only small aggregates composed of less than 5 parallel rods. The modified CNC exhibited slight agglomeration, the rod-like modified particles seemed to form small groups of CNC, organized in parallel, which might be linked to the remaining hydroxyl groups on the CNC surface. We took into consideration this agglomeration in the quantification for the size of the CNC particles (**Table 1**). PGMA-grafted CNC could not be observed by TEM due to the immediate agglomeration of the CNC on the TEM grids after solvent evaporation. Therefore, we used the DLS measurements of Le Gars et al. (2020) [25] in order to compare the hydrodynamic diameter of CNC before and after compatibilization. CNC-g-PGMA exhibited better dispersion in acetone in comparison to the esterified CNCs.

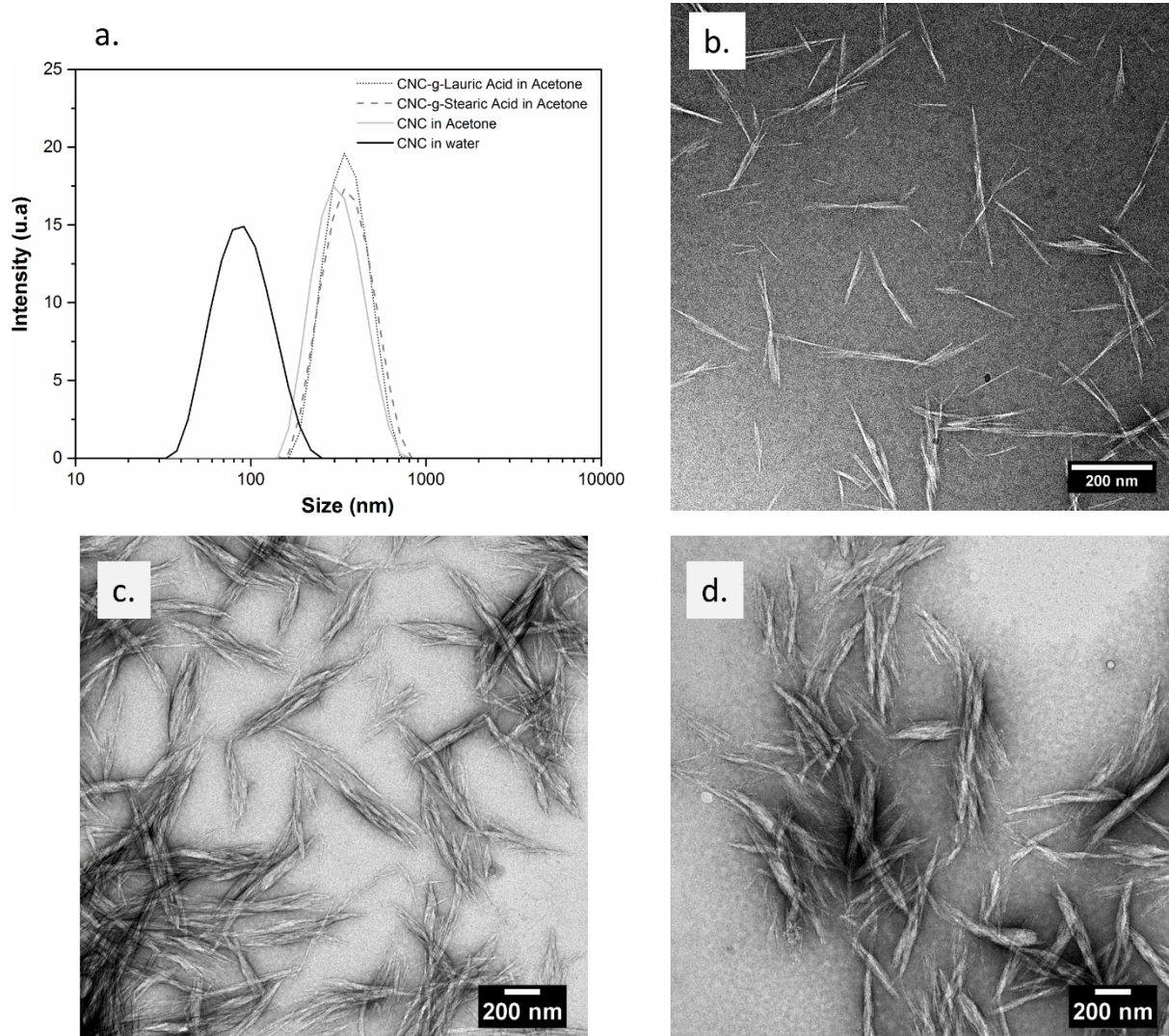


Figure 2. (a) DLS curves of unmodified CNC in water and acetone, and modified CNC in acetone. TEM images of (b) unmodified CNC in water, (c) CNC-g-lauric acid in acetone, and (d) CNC-g-stearic acid in acetone.

The aspect ratio [40], the nature of the bonds linking the particles [4], and the particles orientation [41] are critical parameters determining the percolation threshold in the matrix. Favier et al. (1997) [7] introduced the following relationship for the calculation of the geometrical percolation threshold of CNC for random orientation:

$$V_{rc} = \frac{0.7}{L/w}, \quad \text{Equation (1)}$$

where V_{rc} is the critical volume of percolation, and L and w the length and diameter of the CNC (aspect ratio = L/w). V_{rc} and the corresponding theoretical mass percentage for geometric percolation are presented in **Table 1**. The percolation threshold of the surface grafted CNC was higher than that of the pristine CNC. The dispersion of neat and surface-grafted CNC particles after their incorporation in the PLA matrix was analyzed by observation of the cryofracture

surfaces thanks to SEM measurements. Cross-sections are in **Figure 3a**. Neat PLA showed typical a regular and uniform cross-section due to brittle fracture. **Figure 3b** shows the cross-section of a sample containing 10 wt.% CNC. An increase of coarseness and aggregations can be noticed due to low adhesion between CNC and PLA, as inferred from the cavities observed at the interface. CNC aggregated and the size of the majority of the aggregates was around 4 μm .

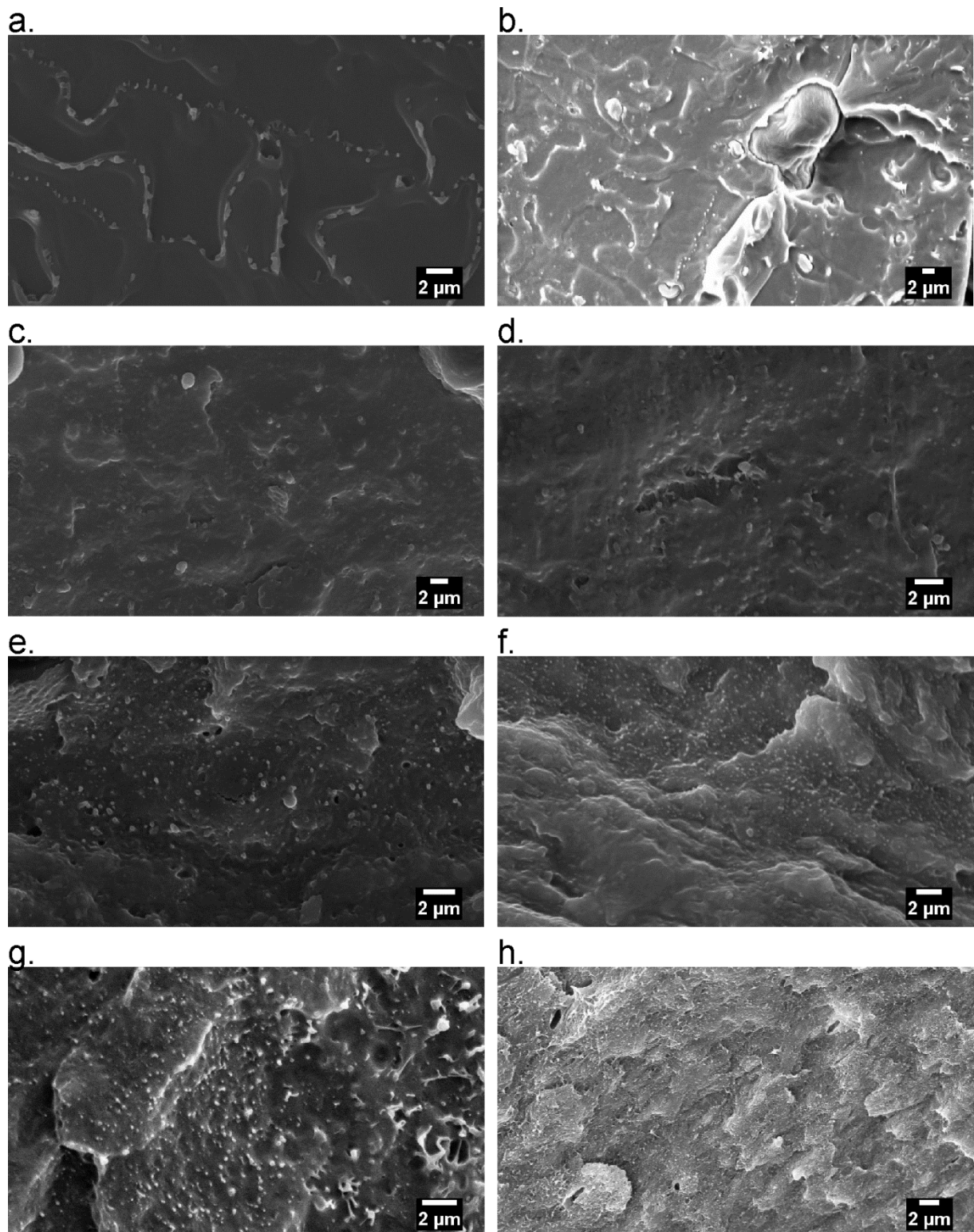


Figure 3. SEM micrographs showing cryo-fractured cross-sections of PLA films containing (a) neat PLA, (b) 10 wt.% CNC, (c) 5 wt.% CNC-g-lauric acid, (d) 10 wt.% CNC-g-lauric acid, (e) 30 wt.% CNC-g-lauric acid, (f) 50 wt.% CNC-g-lauric acid, (g) 10 wt.% CNC-g-stearic acid, (h) 30 wt.% CNC-g-stearic acid. Scale bars represent 2 μm .

In comparison to the PLA/CNC composites, optical inspection of nanocomposites containing surface-modified CNC (see photos in supporting information) showed fully transparent and shiny films, even at high inclusion concentration. **Figures 3c-f** show SEM micrographs of PLA/CNC-g-lauric acid nanocomposites. No CNC-g-lauric acid aggregates were observed. However, it can be noticed the presence of spherical particles when the CNC-g-lauric acid contents increased. This aspect has been previously described as a sign of good dispersion of CNC particles in a chemically compatible matrix [42]. The sample containing CNC-g-stearic acid showed high similarities with CNC-g-lauric acid, as can be seen in **Figures 3g-h**. Consequently, the length of the grafted chain (12 vs. 18-carbon atom chain for lauric and stearic acid respectively) did not seem to influence the morphology nor the dispersion state of the CNC particles within the PLA matrix.

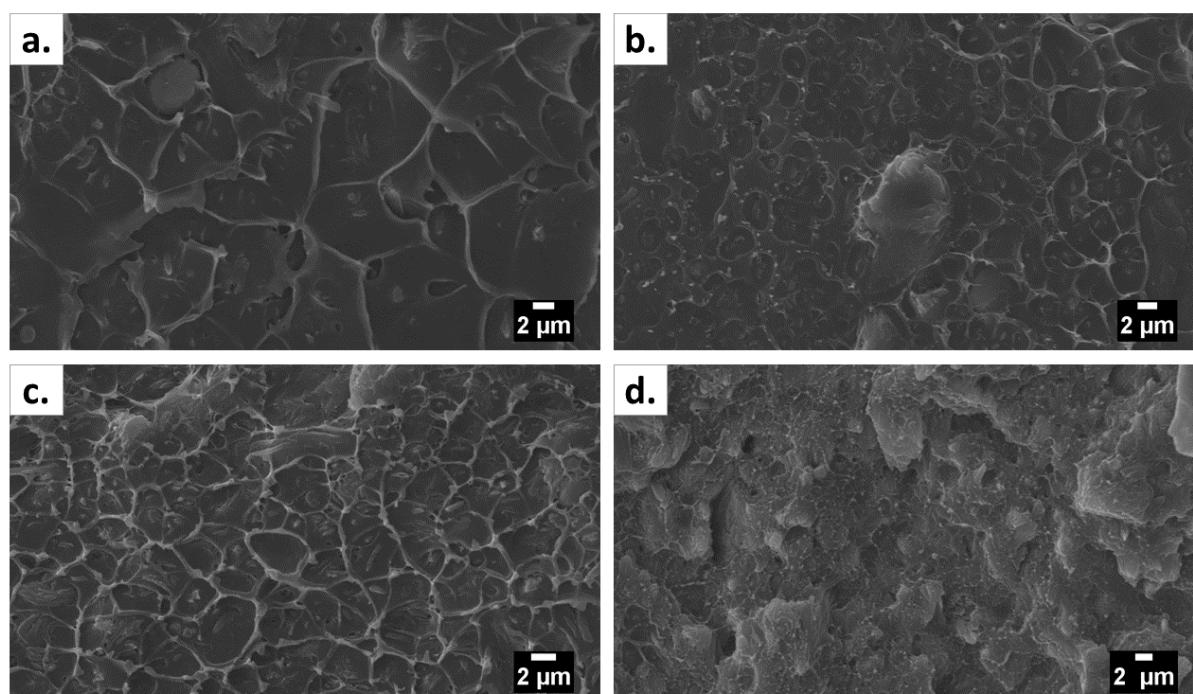


Figure 4. SEM micrographs showing cryofractured cross-sections of PLA/CNC-g-PGMA films containing (a) 2 wt.% (b) 5 wt.% (c) 10 wt.% and (d) 30 wt.%. Scale bars represent 2 μm .

Figure 4 presents the cross-sections of the obtained nanocomposites containing CNC-g-PGMA. SEM micrographs show small aggregates and a distinguishable network-shaped structure, which became predominant as the filler amount increased. This architecture might be caused by crosslinking, because PGMA carries highly reactive pendant epoxy functions. Crosslinking could generate a 3-D network either between the CNC-g-PGMA particles [25], or between PGMA and PLA because of a probable reaction between the PLA hydroxyl groups and the PGMA epoxy groups. This type of reaction was already observed in similar systems [43]. The morphology of CNC-g-PGMA was characterized by Le Gars et al. (2020) [25]. The samples presented a homogenous dispersion of the CNC-PGMA structures and no signs of decohesion at interfaces.

The resolution of the SEM experiment was not enough to observe nanometric particles; therefore, TEM experiments were carried out. Because of the similarity of the morphology of PLA/CNC-g-lauric acid and PLA/CNC-g-stearic acid, the TEM observations were only conducted on the PLA/CNC-g-lauric acid and PLA/CNC-g-PGMA samples. The results are presented in **Figure 5**. **Figure 5a** shows that neat CNC formed large aggregates (around 4 μm), which is consistent with the SEM observations (**Figure 3**). In addition to these large aggregates, small structures of approximately 1 μm length were observed, showing a certain efficiency of dispersion of the casting procedure. Both CNC-g-PGMA (**Figure 5b-c**) and CNC-g-lauric acid (**Figure 5d-f**) particles showed far better dispersion and distribution in the PLA matrix compared to the reference (**Figure 5a**) and very homogeneous dispersion of CNC-g-lauric acid even at very high concentration. The dark zones with a typical size between 0.5 and 3 μm in the PLA/CNC-g-PGMA composites (**Figure 5b-c**) were attributed to crosslinked clusters of CNC-g-PGMA and the contrast in properties between PLA and PGMA. The inclusion concentration of the grafted particles was calculated with respect to the quantity of CNC. Therefore the 30 wt.% CNC-g-PGMA samples contained 54 wt.% PLA, 23 wt.% CNC and 23 wt.% PGMA. Attentive observation of the PGMA phase showed that CNC were more

concentrated inside PGMA than in PLA. This was most probable caused by the crosslinking of CNCs over PGMA bridges.

In conclusion, we created two different morphologies, the first one exhibited a homogeneous dispersion of CNC grafted with fatty acids in PLA, while CNC-g-PGMA showed phase separation with a higher concentration of CNC in a PGMA phase. However, both phases were able to crosslink among each other and with PLA. In the supporting information, thermograms showing an endothermic peak at sample thermocompression temperature are shown. We attributed this peak to the crosslinking reaction. It was only observed at the first heating run.

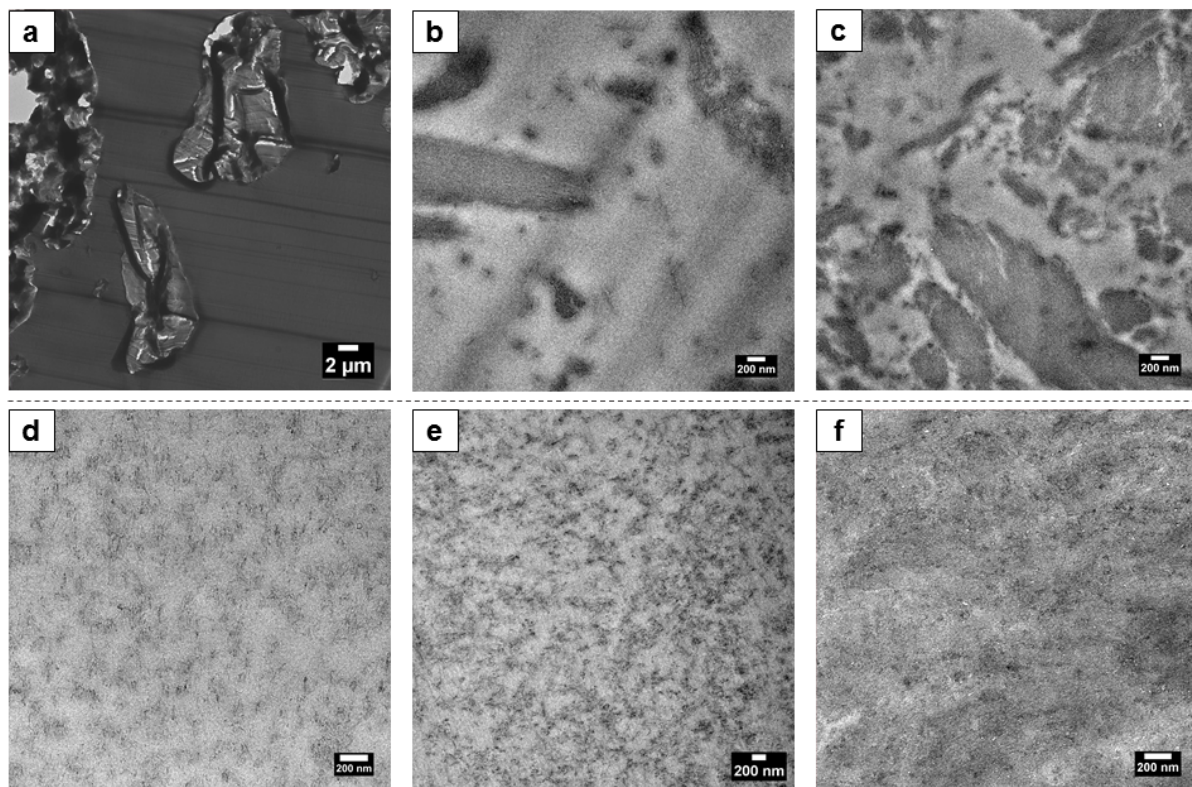


Figure 5. TEM images distribution and dispersion of PLA based composites containing (a) 10 wt.% unmodified-CNC (b) 10 wt.% CNC-g-PGMA (c) 30 wt.% CNC-g-PGMA (d) 10 wt.% CNC-g-lauric acid (e) 30 wt.% CNC-g-lauric acid (f) 50 wt.% CNC-g-lauric acid.

3.3. Thermo-mechanical properties of PLA/CNC nanocomposites

3.3.1. Analysis of the relaxation properties at the glass transition

The effect and properties of the interface between compatibilized nanoparticles and polymer matrix is largely discussed in literature. The segmental relaxation of macromolecular chains near the nanoparticle surfaces can be impacted and cause a behavior different from the bulk properties. Because the nanoparticles develop an important surface, the result of these changes can be observed at a macroscopic scale, for example by a shift of the glass transition temperature [44-47]. A shift of T_g to higher temperatures can be attributed to the presence of wettable surfaces, whereas the shift to lower temperatures would be characteristic of non-wetted surfaces; no change can be expected for weak [44, 48]. We used TM-DSC as a dynamic analysis method without load to characterize the glass transition and relaxation of PLA/CNC nanocomposites with or without surface grafting.

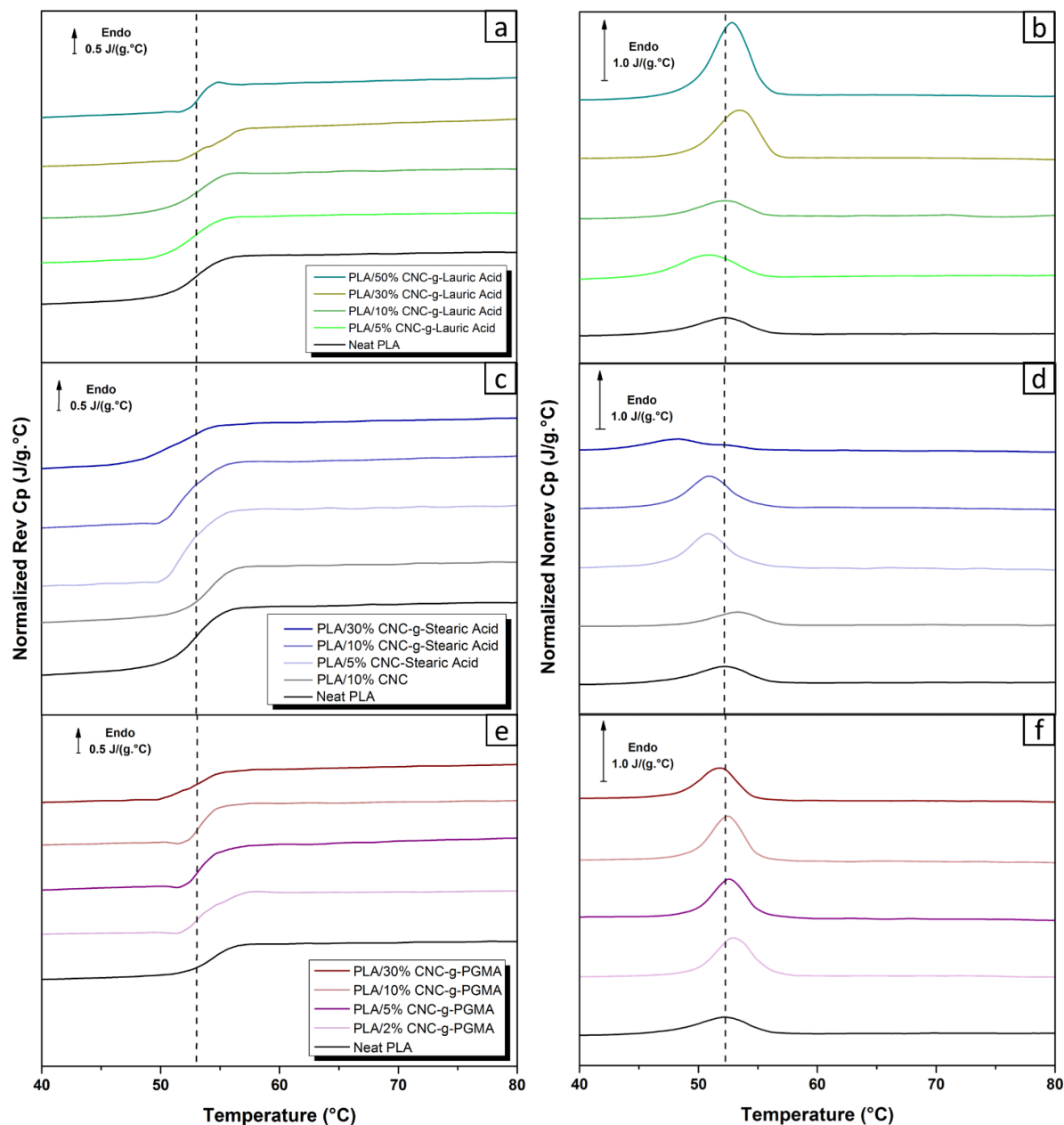


Figure 6. TM-DSC curves displaying reversing and non-reversing normalized C_p in the glass transition region for PLA/CNC nanocomposites.

The TM-DSC curves, presented in **Figure 6**, show the glass transition region of PLA and its nanocomposites, displaying the reversing and non-reversing heat capacity curves obtained using Reading's method [49]. A small overshoot is observed in some samples on the low temperature side of the glass transition. This phenomenon can be explained by a kinetic imbalance caused by very high samples cooling rates (quenching after heat treatment of the films to room temperature) and slow heating rate during the analysis ($2\text{ }^\circ\text{C min}^{-1}$). The observed

values of the T_g measured at the half-height of the glass transition step in **Figure 6** are given in **Table 2**. TM-DSC is a dynamic measurement, therefore the dynamic glass transition temperature (T_α) can be observed as the peak of the non-reversing C_p signal (**Figure 6b,d,f**). It shifted a few degrees towards lower temperatures for the PLA/CNC-g-stearic acid nanocomposites, which indicated weak interactions between PLA and the CNC surface combined with plasticization of the PLA by stearic acid. There seems to be a phase separation at 30 wt.% of CNC-g-stearic acid, where a peak in the non-reversing C_p is found at approximately 48 °C and a second one at 53 °C, the latter corresponding to the T_α of the bulk PLA. In the case of PLA/CNC-g-lauric acid nanocomposites, the position of T_α increased slightly to higher temperatures. This would be still indicative of weak but wetting interactions [44]. The width of the non-reversing C_p peaks increased, which could be also indicative of weak, but existing interactions between CNC surfaces and PLA inducing higher heterogeneity of relaxation times during the glass transition. The CNC-g-PGMA also caused a small reduction of the T_α , which might be caused by the PGMA. The measurement of the T_g of PGMA polymerized with the protocol applied for CNC grafting amounted to 56 °C (TM-DSC curves are given in the supporting information). In this case, the width of the non-reversing C_p peaks was constant, which would indicate that possible impacts of the PLA-PGMA crosslinking cannot be observed by TM-DSC. This is coherent with the observation by TEM (**Figure 5b,c**) showing that the CNC are more concentrated in the PGMA phase than in the PLA.

The heat capacity step ΔC_p was measured at the glass transition (**Table 2**). The value of the neat PLA was very similar to the value reported in the literature for a completely amorphous PLA, 0.51 J/(g °C), although the authors used a different type of PLA [50, 51]. Within the limits of uncertainties, no clear changes in ΔC_p could be observed, so we can conclude that all the samples were amorphous.

Table 2. Glass transition $T_{g,mid}$ (measured at mid-point), T_{α} (measured at the peak of the non-reversing signal), ΔC_p (heat capacity step), and normalized heat capacity step of PLA and PLA/CNC nanocomposites

	CNC Content (wt. %)	$T_{g,mid}$ (°C)	T_{α} (°C)	ΔC_p (J/(g.°C))	Normalized ΔC_p (J/(g.°C))
PLA/ CNC	0	53 ± 1	52	0.464 ± 0.02	0.464
	10	54	53	0.378	0.42
PLA/CNC-g-lauric acid	5	53	51	0.434	0.457
	10	53	52	0.422	0.467
	30	54	53	0.334	0.476
	50	53	53	0.279	0.558
PLA/CNC-g-stearic acid	5	52	51	0.517	0.544
	10	52	51	0.446	0.496
	30	52	48	0.329	0.469
PLA/CNC-g-PGMA	2	54	52	0.458	0.467
	5	53	53	0.480	0.506
	10	53	52	0.449	0.499
	30	53	52	0.377	0.538

3.3.2. Analysis of the thermo-mechanical properties and CNC percolation

The relaxation properties of the nanocomposites under mechanical load were analyzed using DMA. Because of the morphological similarity of CNC-g-stearic acid and CNC-g-lauric acid and the small shift of T_{α} to higher temperatures, only the latter type of esterified CNC was investigated in further detail and compared to the effects obtained by crosslinking of PLA and CNC-g-PGMA. **Figure 7** summarizes typical experimental curves for the storage modulus and the dissipation factor (tan delta).

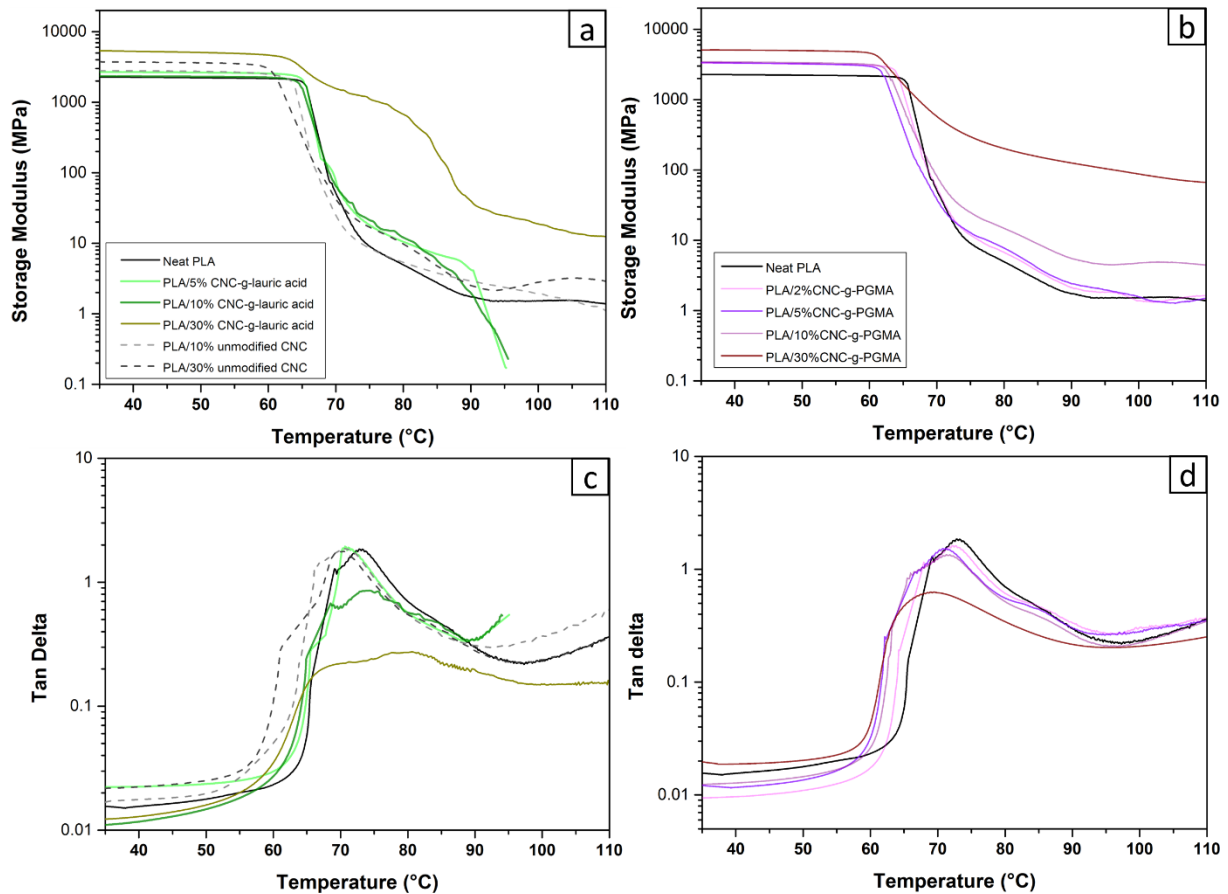


Figure 7. Storage modulus E' and tan delta as a function of temperature for PLA/CNC-g-lauric acid (left) and PLA/CNC-g-PGMA (right) nanocomposites.

The DMA curves of PLA confirmed the amorphous character and the absence of crystallization which would cause an increase in the storage modulus in the rubbery plateau. Loading PLA with 10 wt.% of CNC had no observable impact on the storage moduli of the materials, while loading with 30 wt.% CNC increased slightly the moduli (**Figure 7a,c**). The PLA/CNC-g-lauric acid nanocomposites (**Figure 7a,c**) showed no differences in the behavior of the glass transition compared to neat PLA, except for the CNC-g-lauric acid concentration of 30 wt.%. For this content, the glass transition seemed to be composed of two steps: the first drop started at $T_{\text{onset}} = 63$ °C, which is compatible with the dynamic glass transition of PLA, the second drop started at $T_{\text{onset}} = 76$ °C. We suggest that this might be caused by two distinct phases where the first step would concern bulk PLA and the second would be related to an amorphous phase which is hindered in its relaxation by the presence of the nanoparticles with attractive, wetting surfaces

[44]. The result is coherent with the MT-DSC data (**Figure 6b**), which showed broadening of the glass transition region at quantities of CNC higher than the geometric percolation threshold (here 9 wt. %, **Table 1**). It was also observed by other authors, that the inclusion of CNC at concentrations higher than the percolation threshold induces broadening of the glass transition [33, 52, 53]. **Figure 7b, d** shows the DMA curves of the PLA/CNC-g-PGMA nanocomposites. The onset of the glass transition decreased linearly with increasing concentration of the CNC-g-PGMA (**Figure 7b,d**), but the effect was very small, as already observed in (**Figure 6f**). The small shift of T_{α} could be indicative of a weak interaction between PGMA and PLA or of the impact of PGMA to the overall behavior. Because of the overlap of the glass transition region of PLA and PGMA, the individual T_{α} of each polymer could not be distinguished.

Figure 7 shows the increase of the elastic modulus of the PLA nanocomposites in the glassy and in the rubbery plateau with increasing volume fraction of the compatibilized CNC. The values for the glassy plateau were taken at 40 °C. Because PLA/CNC-g-lauric acid nanocomposites flowed shortly after the glass transition, the values were taken in the range of 80 to 85 °C, which overestimated the effective modulus of the rubbery plateau. The inclusion of 30 wt.% (27.6 vol.%) of CNC-g-lauric acid improved the glassy modulus of the materials by a factor 2.4 and the rubbery modulus by a factor 150. Surface grafted CNC are therefore a performing reinforcement of PLA. The inclusion of CNC-g-PGMA in PLA resulted in smaller, but still important reinforcement factors. The glassy modulus increased by a factor 2.2 and the rubbery modulus by a factor around 40. A comparative figure summarizing the results can be found in the supporting information. Very encouraging results of PLA/CNC-g-PGMA nanocomposites showed that a high rubbery storage modulus can be maintained up to 110 °C which indicated an improvement of the heat deflexion stability of PLA. This behavior can be attributed to the crosslinking of CNC-g-PGMA and PLA.

Although surface modification of CNC particles and its influence on the mechanical properties of nanocomposites is a subject of great interest, the impact of the surface modification on the

reinforcing effect, stiffness and formation of a percolation network within a matrix is still scarcely discussed. The elastic modulus can be predicted using different models, such as the Halpin-Tsai model classically used for short-fiber composites [54] or the Ouali model for percolating fillers [9]. In both models the modulus of the filler is assumed to be much higher than the modulus of the matrix, i.e. $E_m \ll E_f$. The Halpin-Tsai model is generally used to describe the modulus of composites using short fibers without interaction and oriented parallel to the tensile direction [54]. The polymer matrix is considered to be an elastic continuum, with a known modulus (E_m) and Poisson ratio (ν_m). This model applies for non-percolating systems:[55]

$$E_c = E_m \frac{1 + \{(k_E - 1)v_r / [1 + (k_E - 1)(E_m/E_f)]\}}{1 - v_r / [1 + (k_E - 1)(E_m/E_f)]}, \quad \text{Equation (2)}$$

with E being the elastic modulus, and the subscripts m, f and c referring to matrix, filler and composite, respectively, v_r the filler volume fraction, k_E is the Einstein coefficient, given by the equation 3:

$$k_E = \frac{\rho^2}{15 \ln(\frac{\rho}{2})}, \quad \text{Equation (3)}$$

where ρ is the aspect ratio, determined to be 12 for modified CNC and 20 for unmodified CNC (Table 1).

The Ouali model is based on the series-parallel model of Takayanagi et al. (1964) [56] and includes percolation effects on the reinforcement of the matrix moduli. It takes into consideration three phases, *i.e.* the matrix, the percolating network and the non-percolating filler phase [9]. The elastic modulus of the composite (E_c) is obtained following the equation:

$$E_c = \frac{(1 - 2\Psi + \Psi v_r)E_m E_f + (1 - v_r)\Psi E_f^2}{(1 - v_r)E_f + (v_r - \Psi)E_m}, \quad \text{Equation (4)}$$

where Ψ is an adjustable parameter that is associated to the percolated filler fraction, given by:

$$\Psi = 0 \quad \text{for } v_r < v_{rc}, \quad \text{Equation (5)}$$

and

$$\Psi = v_r \left(\frac{v_r - v_{rc}}{1 - v_{rc}} \right)^b \quad \text{for } v_r > v_{rc}, \quad \text{Equation (6)}$$

where b is the critical percolation exponent, corresponding to the value of 0.4 for a 3-D network, according to Stauffer & Aharony (1992) [57] and v_{rc} is the percolation threshold.

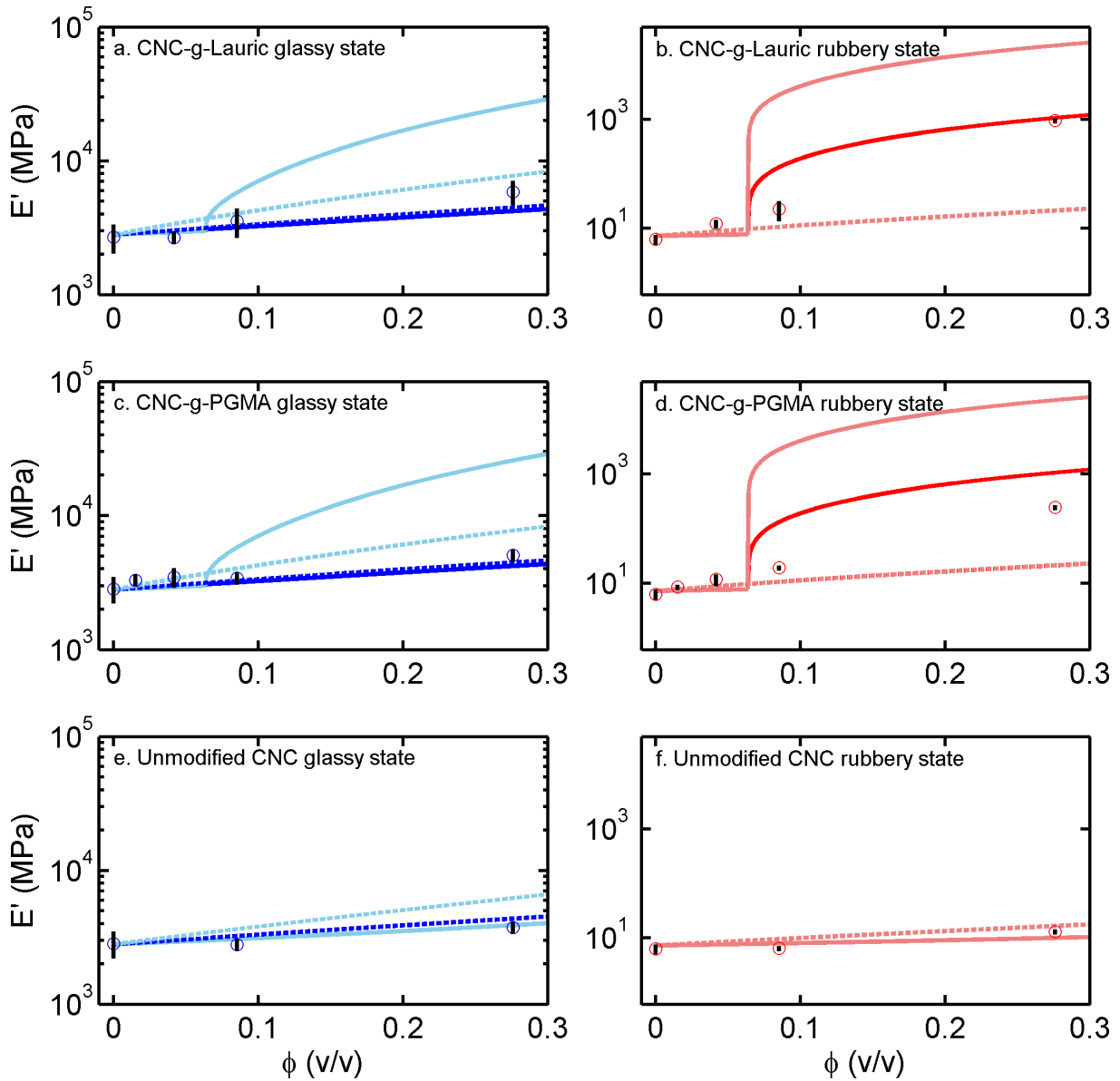


Figure 8. Logarithm of storage modulus, for PLA and PLA/CNC-g-lauric acid and PLA/CNC-g-PGMA films, in the glassy (40 °C) and rubbery (80-85 °C) state. Comparisons between measured data (points) and data predicted by the Halpin Tsai model (dashed line) and the Ouali model (full line). Aspect ratio was taken equal to 11.6 for grafted CNC and 2.5 for pristine CNC. Light blue and red represent models with $E_f=150$ GPa and dark blue and red $E_f = 7$ GPa. The two calculations of the Halpin-Tsai model in the rubbery state superposed.

Figure 8 shows the fit of the Halpin-Tsai and the Ouali models to the experimental data in the glassy (**Figure 8a,c**) and the rubbery region (**Figure 8b,d**) as a function of the CNC volume fraction. The E_f value of the CNC and its network are difficult to determine, but different values

are given in the literature. We show here the computed model results assuming $E_f = 150$ GPa [7]. This value was calculated from the C-bonds in the CNC particles [58]. **Figure 8** presents furthermore model calculations assuming $E_f = 7$ GPa [59]. This value would correspond to the modulus of a CNC sheet. Both moduli were set independent from temperature.

Assuming $E_f = 150$ GPa [7], the Halpin-Tsai model described satisfyingly the evolution of E' in the glassy region of the PLA/CNC-g-lauric acid and PLA/CNC-g-PGMA nanocomposites (**Figure 8a,c**). The addition of CNC at low concentrations (5 and 10 wt.%) had no significant effect considering the uncertainties of the measurements (an error of 3 % on thickness results in an error of 10 % on the modulus). Assuming $E_f = 7$ GPa [59], the Halpin-Tsai model failed to describe the evolution of the nanocomposites' moduli with increasing volume fraction, although the model was not very sensitive to the E_f value (calculations with different values are shown in the supporting information). We concluded that this lack of sensitivity is caused by the relatively small difference of E' between PLA and CNC in the glassy plateau. In the rubbery plateau (**Figure 8b,d**), the Halpin-Tsai model failed to describe the experimental data whatever the assumed E_f value. There was a clear change of E' between 8.51 and 27.6 vol% of grafted CNC, which would be indicative of the percolation of the CNC network. Similar conclusions were already drawn [8], when they noticed a higher reinforcement of the materials than predicted. As discussed before in the morphology section, the percolation threshold of CNC-g-lauric acid amounted to 6 vol. % and the one of neat CNC to 3.3 vol% (**Table 1**).

The Ouali model prediction was calculated in the glassy and the rubbery plateau using the E_f value of CNC single particles and the one of CNC sheets (**Figure 8b,d**). Clearly, the Ouali model failed to describe experimental data in the glassy plateau. We suppose that the small differences in modulus between CNC and PLA are the reason of that. The Ouali percolation model is indeed highly dependent on the E_f value, and a change in the aspect ratio has no impact on modulus once percolation is reached (examples are shown in the supporting information). In the rubbery plateau, the Ouali model using $E_f = 7$ GPa came closer to experimental values of

PLA/CNC-g-lauric acid and PLA/CNC-g-PGMA nanocomposites. In the percolation theory, the filler-filler interactions are important. Dufresne (2012) [4] proposed, based on the work of Favier et al. (1995) [8], that the percolation network of CNC is bridged by the strong interactions between particles over hydrogen bonds. Modification of the hydroxyl groups on the CNC surface would diminish the capability to form inter-particle hydrogen bonds and therefore shift the percolation threshold towards higher contents [12]. A possible shift of the percolation to higher values than the one predicted in **Table 1** cannot be inferred due to the lack of experimental data. The surface modification would also diminish the capacity to establish H-bonds between single CNC and therefore weaken the percolated network. As a consequence, the observed reinforcement effect is much lower than predicted. This would explain why the hypothesis $E_f = 7$ GPa came closer to the experimental values, especially to those of the PLA/CNC-g-lauric acid nanocomposites. At low CNC content, the Ouali model failed to predict observed evolution, because the matrix-filler interactions, filler orientation and dispersion are neglected in the calculation of the overall mechanical properties [10]. The rubbery modulus of the PLA/CNC samples was lower than that of the PLA/CNC-g-lauric acid and PLA/CNC-g-PGMA samples (**Figure 8b**), which shows the impact of the surface compatibilization on the elastic modulus. The rubbery moduli of the compatibilized systems increased nearly linearly with the filler volume fraction. We suggest that this is caused by the weak positive interaction between CNC-g-lauric acid surfaces and PLA, which weakens the CNC/CNC percolating network but gives rise to stress transfer. The PLA/CNC-g-PGMA samples had lower elastic moduli compared to the PLA/CNC-g-lauric acid nanocomposites. In this case, CNC were concentrated in the PGMA phase (**Figure 5b,c**), which could decrease further the strength or even prevent the establishment of a percolated CNC network. However, stress transfer between PGMA and CNC would be increased and the system might be better described by a blend morphology of a reinforced PGMA and a PLA phase.

4. Conclusion

Homogeneously dispersed amorphous bio-nanocomposites of polylactide and surface-grafted cellulose nanocrystals were successfully produced by casting and compression molding with concentrations up to 50 wt. % CNC particles. Two types of surface compatibilizer (fatty acids and PGMA with reactive end-groups) were compared and their performance investigated in terms of type of interaction with the PLA matrix and viscoelastic moduli below and above glass transition. The underlying mechanisms were analyzed using the Ouali model for percolated systems and the Halpin-Tsai model for composites with short fibers. The epoxy groups of CNC-g-PGMA reacted among themselves and with PLA, which formed a phase separated system. This system did not percolate and its mechanical performance was governed by the covalent filler/matrix coupling. The CNC surface compatibilizing with fatty acids, which are abundant, non-toxic, biobased and biodegradable molecules generated only in weak CNC/PLA interactions. Nevertheless, the fatty acids were efficient dispersants of CNC in the matrix and the gain in the rubbery elastic modulus was very important. This could be ascribed to percolation, although the strength of the percolated network was imparted by the surface grafting because it hindered of the establishment of inter-CNC H-bonds. We conclude that for efficient surface compatibilization of CNC, the establishment of only weak CNC/PLA interactions can result in performing materials. In our case, the system using fatty acids and a quite simple and scalable surface grafting method complying with several principles of green chemistry was the most efficient. It matched best with the overall aim of developing materials with decreased environmental impact.

Acknowledgments

The authors acknowledge financial support from the French National Research Agency (ANR) for the national research project ANR-16-CE08-0040 – GASP.

Supporting Information

Supporting Information is available from the Wiley Online Library or from the author.

References

- [1] T. Owoyokun, C.M.P. Berumen, A.M. Luevanos, L. Cantu, A.C.L. Cenicerros, Cellulose Nanocrystals: Obtaining and Sources of a Promising Bionanomaterial for Advanced Applications, *Biointerface Res. Appl. Chem.*, 11 (2021) 11797-11816. 10.33263/briac114.1179711816.
- [2] K. Dhali, M. Ghasemlou, F. Daver, P. Cass, B. Adhikari, A review of nanocellulose as a new material towards environmental sustainability, *Sci. Total Environ.*, 775 (2021) 24. 10.1016/j.scitotenv.2021.145871.
- [3] A. Šturcová, G.R. Davies, S.J. Eichhorn, Elastic modulus and stress-transfer properties of tunicate cellulose whiskers, *Biomacromolecules*, 6 (2005) 1055-1061. 10.1021/bm049291k.
- [4] A. Dufresne, *Nanocellulose: from nature to high performance tailored materials*, de Gruyter, Berlin/Boston, 2012.
- [5] R. Rusli, S.J. Eichhorn, Determination of the stiffness of cellulose nanowhiskers and the fiber-matrix interface in a nanocomposite using Raman spectroscopy, *Appl. Phys. Lett.*, 93 (2008) 033111. <https://doi.org/10.1063/1.2963491>.
- [6] H. Kargarzadeh, M. Mariano, J. Huang, N. Lin, I. Ahmad, A. Dufresne, S. Thomas, Recent developments on nanocellulose reinforced polymer nanocomposites: A review, *Polymer*, 132 (2017) 368-393. <https://doi.org/10.1016/j.polymer.2017.09.043>.
- [7] V. Favier, G.R. Canova, S.C. Shrivastava, J.Y. Cavaille, Mechanical percolation in cellulose whisker nanocomposites, *Polym. Eng. Sci.*, 37 (1997) 1732-1739.
- [8] V. Favier, H. Chanzy, J.Y. Cavaille, Polymer Nanocomposites Reinforced by Cellulose Whiskers, *Macromolecules*, 28 (1995) 6365-6367. 10.1021/ma00122a053.
- [9] N. Ouali, J. Cavaillé, J. Perez, Elastic, viscoelastic and plastic behavior of multiphase polymer blends, *Plastics, Rubber and Composites Processing and Applications (UK)*, 16 (1991) 55-60.
- [10] C. Miao, W.Y. Hamad, Critical insights into the reinforcement potential of cellulose nanocrystals in polymer nanocomposites, *Curr. Opin. Solid State Mater. Sci.*, 23 (2019) 100761. <https://doi.org/10.1016/j.cossms.2019.06.005>.
- [11] W. Abdallah, M.R. Kamal, Cellulose Nanocrystals: Particles and Polymer Nanocomposites, in: *Processing of Polymer Nanocomposites*, Hanser, 2019, pp. 395-434.
- [12] G. Siqueira, J. Bras, A. Dufresne, Cellulose whiskers versus microfibrils: influence of the nature of the nanoparticle and its surface functionalization on the thermal and mechanical properties of nanocomposites, *Biomacromolecules*, 10 (2009) 425-432. <https://doi.org/10.1021/bm801193d>.
- [13] V. Ducruet, S. Domenek, Characteristics and applications of poly(lactic acid) in: S. Kalia, L. Averous (Eds.) *Biodegradable and Bio-based Polymers: Environmental and Biomedical Applications*, Scrivener Publishing LLC, Beverly, MA 2015, pp. 171-224.
- [14] S. Domenek, S. Fernandes-Nassar, V. Ducruet, Rheology, Mechanical Properties, and Barrier Properties of Poly(lactic acid), in: M.L. Di Lorenzo, R. Androsch (Eds.) *Synthesis, Structure and Properties of Poly(lactic acid)*, Springer International Publishing, Cham, 2018, pp. 303-341.
- [15] S. Saeidlou, M.A. Huneault, H. Li, C.B. Park, Poly(lactic acid) Crystallization, *Prog. Polym. Sci.*, 37 (2012) 1657-1677. <https://doi.org/10.1016/j.progpolymsci.2012.07.005>.
- [16] E. Vatansever, D. Arslan, M. Nofar, Polylactide cellulose-based nanocomposites, *Int. J. Biol. Macromol.*, 137 (2019) 912-938. 10.1016/j.ijbiomac.2019.06.205.
- [17] E. Espino-Perez, S. Domenek, N. Belgacem, C. Sillard, J. Bras, Green Process for Chemical Functionalization of Nanocellulose with Carboxylic Acids, *Biomacromolecules*, 15 (2014) 5441-4560. 10.1021/bm5013458.

- [18] D. Rigotti, R. Checchetto, S. Tarter, D. Caretti, M. Rizzuto, L. Fambri, A. Pegoretti, Poly(lactic acid)-lauryl functionalized nanocellulose nanocomposites: Microstructural, thermo-mechanical and gas transport properties, *Express Polym. Lett.*, 13 (2019). <https://doi.org/10.3144/expresspolymlett.2019.75>.
- [19] J. Shojaeiarani, D.S. Bajwa, K. Hartman, Esterified cellulose nanocrystals as reinforcement in poly (lactic acid) nanocomposites, *Cellulose*, 26 (2019) 2349-2362.
- [20] S. Spinella, C.d. Samuel, J.-M. Raquez, S.A. McCallum, R. Gross, P. Dubois, Green and efficient synthesis of dispersible cellulose nanocrystals in biobased polyesters for engineering applications, *ACS Sustain. Chem. Eng.*, 4 (2016) 2517-2527. <https://doi.org/10.1021/acssuschemeng.5b01611>.
- [21] B. Braun, J.R. Dorgan, L.O. Hollingsworth, Supra-Molecular EcoBioNanocomposites Based on Poly(lactide) and Cellulosic Nanowhiskers: Synthesis and Properties, *Biomacromolecules*, 13 (2012) 2013-2019. 10.1021/bm300149w.
- [22] G. Lo Re, S. Spinella, A. Boujemaoui, F. Vilaseca, P.T. Larsson, F. Adås, L.A. Berglund, Poly (ϵ -caprolactone) Biocomposites Based on Acetylated Cellulose Fibers and Wet Compounding for Improved Mechanical Performance, *ACS Sustain. Chem. Eng.*, 6 (2018) 6753-6760.
- [23] Y. Habibi, S. Aouadi, J.M. Raquez, P. Dubois, Effects of interfacial stereocomplexation in cellulose nanocrystal-filled poly(lactide) nanocomposites, *Cellulose*, 20 (2013) 2877-2885. 10.1007/s10570-013-0058-5.
- [24] H. Wu, S. Nagarajan, L. Zhou, Y. Duan, J. Zhang, Synthesis and characterization of cellulose nanocrystal-graft-poly (D-lactide) and its nanocomposite with poly (L-lactide), *Polymer*, 103 (2016) 365-375. <https://doi.org/10.1016/j.polymer.2016.09.070>.
- [25] M. Le Gars, J. Bras, H. Salmi-Mani, M. Ji, D. Dragoë, H. Faraj, S. Domenek, N. Belgacem, P. Roger, Polymerization of glycidyl methacrylate from the surface of cellulose nanocrystals for the elaboration of PLA-based nanocomposites, *Carbohydr. Polym.*, 234 (2020) 115899. <https://doi.org/10.1016/j.carbpol.2020.115899>.
- [26] E. Fortunati, M. Peltzer, I. Armentano, L. Torre, A. Jiménez, J. Kenny, Effects of modified cellulose nanocrystals on the barrier and migration properties of PLA nanobiocomposites, *Carbohydr. Polym.*, 90 (2012) 948-956. <https://doi.org/10.1016/j.carbpol.2012.06.025>.
- [27] L. Petersson, I. Kvien, K. Oksman, Structure and thermal properties of poly(lactic acid)/cellulose whiskers nanocomposite materials, *Compos. Sci. Technol.*, 67 (2007) 2535-2544. 10.1016/j.compscitech.2006.12.012.
- [28] W. Meesorn, A. Shirole, D. Vanhecke, L.M. de Espinosa, C. Weder, A simple and versatile strategy to improve the mechanical properties of polymer nanocomposites with cellulose nanocrystals, *Macromolecules*, 50 (2017) 2364-2374. <https://doi.org/10.1021/acs.macromol.6b02629>.
- [29] M. Nagalakshmaiah, F. Pignon, N. El Kissi, A. Dufresne, Surface adsorption of triblock copolymer (PEO-PPO-PEO) on cellulose nanocrystals and their melt extrusion with polyethylene, *RSC Advances*, 6 (2016) 66224-66232. 10.1039/c6ra11139d.
- [30] K. Gopalan Nair, A. Dufresne, A. Gandini, M.N. Belgacem, Crab shell chitin whiskers reinforced natural rubber nanocomposites. 3. Effect of chemical modification of chitin whiskers, *Biomacromolecules*, 4 (2003) 1835-1842. 10.1021/bm030058g.
- [31] E. Robles, I. Urruzola, J. Labidi, L. Serrano, Surface-modified nano-cellulose as reinforcement in poly (lactic acid) to conform new composites, *Ind. Crops Prod.*, 71 (2015) 44-53. <https://doi.org/10.1016/j.indcrop.2015.03.075>.
- [32] M. Le Gars, P. Roger, N. Belgacem, J. Bras, Role of solvent exchange in dispersion of cellulose nanocrystals and their esterification using fatty acids as solvents, *Cellulose*, 27 (2020) 4319-4336. 10.1007/s10570-020-03101-0.

- [33] E. Espino-Pérez, J. Bras, G. Almeida, C. Plessis, N. Belgacem, P. Perré, S. Domenek, Designed cellulose nanocrystal surface properties for improving barrier properties in polylactide nanocomposites, *Carbohydr. Polym.*, 183 (2018) 267-277. <https://doi.org/10.1016/j.carbpol.2017.12.005>.
- [34] L. Segal, J.J. Creely, A. Martin Jr, C. Conrad, An empirical method for estimating the degree of crystallinity of native cellulose using the X-ray diffractometer, *Text. Res. J.*, 29 (1959) 786-794.
- [35] Q. Beuguel, J.R. Tavares, P.J. Carreau, M.-C. Heuzey, Ultrasonication of spray-and freeze-dried cellulose nanocrystals in water, *J. Colloid Interface Sci.*, 516 (2018) 23-33. <https://doi.org/10.1016/j.jcis.2018.01.035>.
- [36] F. Shafizadeh, A. Bradbury, Thermal degradation of cellulose in air and nitrogen at low temperatures, *J. Appl. Polym. Sci.*, 23 (1979) 1431-1442.
- [37] M. Kumar, S. Mohanty, S. Nayak, M.R. Parvaiz, Effect of glycidyl methacrylate (GMA) on the thermal, mechanical and morphological property of biodegradable PLA/PBAT blend and its nanocomposites, *Bioresour. Technol.*, 101 (2010) 8406-8415. <https://doi.org/10.1016/j.biortech.2010.05.075>.
- [38] Q. Beuguel, J.R. Tavares, P.J. Carreau, M.-C. Heuzey, Rheological behavior of cellulose nanocrystal suspensions in polyethylene glycol, *J. Rheol.*, 62 (2018) 607-618. <https://doi.org/10.1122/1.5010789>.
- [39] C. Bruel, Q. Beuguel, J.R. Tavares, P.J. Carreau, M.C. Heuzey, The apparent structural hydrophobicity of cellulose nanocrystals, *J-For*, 7 (2018) 13-23. <https://publications.polymtl.ca/4126/>
- [40] P.-G. De Gennes, On a relation between percolation theory and the elasticity of gels, *Journal de Physique Lettres*, 37 (1976) 1-2.
- [41] I. Balberg, N. Binenbaum, N. Wagner, Percolation thresholds in the three-dimensional sticks system, *Phys. Rev. Lett.*, 52 (1984) 1465.
- [42] S. Krishna, C.M. Patel, Computational and experimental study of mechanical properties of Nylon 6 nanocomposites reinforced with nanomilled cellulose, *Mech. of Mater.*, 143 (2020) 103318. <https://doi.org/10.1016/j.mechmat.2020.103318>.
- [43] Z.Q. Li, X.D. Zhou, C.H. Pei, Synthesis of PLA-co-PGMA copolymer and its application in the surface modification of bacterial cellulose, *Int. J. Polym. Mater.*, 59 (2010) 725-737. 10.1080/00914037.2010.483214.
- [44] J. Jancar, J.F. Douglas, F.W. Starr, S.K. Kumar, P. Cassagnau, A.J. Lesser, S.S. Sternstein, M.J. Buehler, Current issues in research on structure-property relationships in polymer nanocomposites, *Polymer*, 51 (2010) 3321-3343. 10.1016/j.polymer.2010.04.074.
- [45] Y. Lin, L. Liu, G. Xu, D. Zhang, A. Guan, G. Wu, Interfacial interactions and segmental dynamics of poly (vinyl acetate)/silica nanocomposites, *J. Phys. Chem. C*, 119 (2015) 12956-12966. 10.1021/acs.jpcc.5b01240.
- [46] P. Rittigstein, R.D. Priestley, L.J. Broadbelt, J.M. Torkelson, Model polymer nanocomposites provide an understanding of confinement effects in real nanocomposites, *Nat. Mater.*, 6 (2007) 278-282. 10.1038/nmat1870.
- [47] O. Yousefzade, J. Jeddi, E. Vazirinasab, H. Garmabi, Poly(lactic acid) phase transitions in the presence of nano calcium carbonate: Opposing effect of nanofiller on static and dynamic measurements, *J. Thermoplast. Compos. Mater.*, 32 (2019) 312-327. 10.1177/0892705718759386.
- [48] P. Rittigstein, J.M. Torkelson, Polymer-nanoparticle interfacial interactions in polymer nanocomposites: Confinement effects on glass transition temperature and suppression of physical aging, *J. Polym. Sci. Pt. B-Polym. Phys.*, 44 (2006) 2935-2943. 10.1002/polb.20925.
- [49] A.A. Lacey, D.M. Price, M. Reading, Theory and practice of modulated temperature differential scanning calorimetry, in: *Modulated Temperature Differential Scanning Calorimetry*, Springer, 2006, pp. 1-81.

- [50] X. Monnier, A. Saiter, E. Dargent, Physical aging in PLA through standard DSC and fast scanning calorimetry investigations, *Thermochim. Acta*, 648 (2017) 13-22.
<https://doi.org/10.1016/j.tca.2016.12.006>.
- [51] X. Cao, A. Mohamed, S. Gordon, J. Willett, D. Sessa, DSC study of biodegradable poly (lactic acid) and poly (hydroxy ester ether) blends, *Thermochim. Acta*, 406 (2003) 115-127.
[https://doi.org/10.1016/S0040-6031\(03\)00252-1](https://doi.org/10.1016/S0040-6031(03)00252-1).
- [52] L. Wei, U.P. Agarwal, L. Matuana, R.C. Sabo, N.M. Stark, Performance of high lignin content cellulose nanocrystals in poly(lactic acid), *Polymer*, 135 (2018) 305-313.
<https://doi.org/10.1016/j.polymer.2017.12.039>.
- [53] Y. Yin, L.A. Lucia, L. Pal, X. Jiang, M.A. Hubbe, Lipase-catalyzed laurate esterification of cellulose nanocrystals and their use as reinforcement in PLA composites, *Cellulose*, 27 (2020) 6263-6273.
- [54] J. Halpin, J. Kardos, Moduli of crystalline polymers employing composite theory, *J. Appl. Phys.*, 43 (1972) 2235-2241.
- [55] A.P. Chatterjee, A model for the elastic moduli of three-dimensional fiber networks and nanocomposites, *J. Appl. Phys.*, 100 (2006) 054302. <https://doi.org/10.1063/1.2336088>.
- [56] M. Takayanagi, S. Uemura, S. Minami, Application of equivalent model method to dynamic rheo-optical properties of crystalline polymer, *J. Polym. Sci., Part C: Polym. Symp.*, 5 (1964) 113-122. <https://doi.org/10.1002/polc.5070050111>.
- [57] D. Stauffer, Introduction to percolation theory/Dietrich Stauffer and Amnon Aharony, in, Taylor and Francis, London, 2nd ed., 1992.
- [58] K. Tashiro, M. Kobayashi, Theoretical evaluation of three-dimensional elastic constants of native and regenerated celluloses: Role of hydrogen bonds, *Polymer*, 32 (1991) 1516-1526.
[https://doi.org/10.1016/0032-3861\(91\)90435-L](https://doi.org/10.1016/0032-3861(91)90435-L).
- [59] E. Limousin, I. Rafaniello, T. Schafer, N. Ballard, J.M. Asua, Linking Film Structure and Mechanical Properties in Nanocomposite Films Formed from Dispersions of Cellulose Nanocrystals and Acrylic Latexes, *Langmuir*, 36 (2020) 2052-2062.
10.1021/acs.langmuir.9b03861.

Supporting Information

A comparative study of the thermo-mechanical properties of polylactide/cellulose nanocrystal nanocomposites obtained by two surface compatibilization strategies

Faraj^{1,2}, Cyrille Sollogoub², Alain Guinault², Mathieu Gervais², Julien Bras³, Hanène Salmi⁴,
Philippe Roger⁴, Manon Le Gars³, Sandra Domenek¹

¹Université Paris-Saclay, INRAE, AgroParisTech, UMR SayFood, 91300, Massy, France

²Laboratoire PIMM, Arts et Metiers Institute of Technology, CNRS, Cnam, Hesam Université, 151,
Boulevard de l'Hôpital, F-75013 Paris Cedex, France

³Univ. Grenoble Alpes, CNRS, Grenoble INP, LGP2, F-38000 Grenoble, France

⁴Institut De Chimie Moléculaire Et Des Matériaux d'Orsay, Université Paris-Saclay, CNRS, 91405
Orsay, France

Corresponding author: Sandra Domenek, UMR SayFood (Université Paris-Saclay, INRAE,
AgroParisTech), 1 rue des Olympiades, 91300 Massy, France; sandra.domenek@agroparistech.fr

Particle size distribution of CNC powders

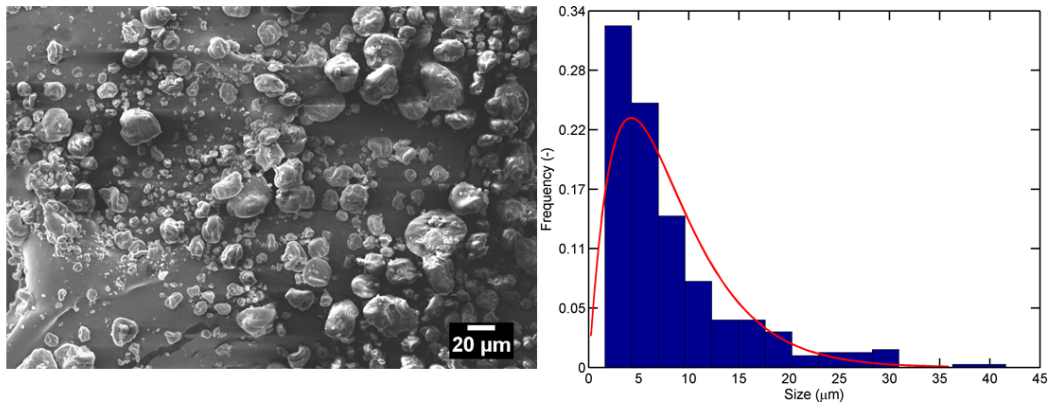


Fig. S.1 Micrograph of commercially purchased CNC (Celluforce) aggregated particles with an average interval size of [2.00- 4.00], with a histogram of CNC particle size distribution based on SEM micrograph.

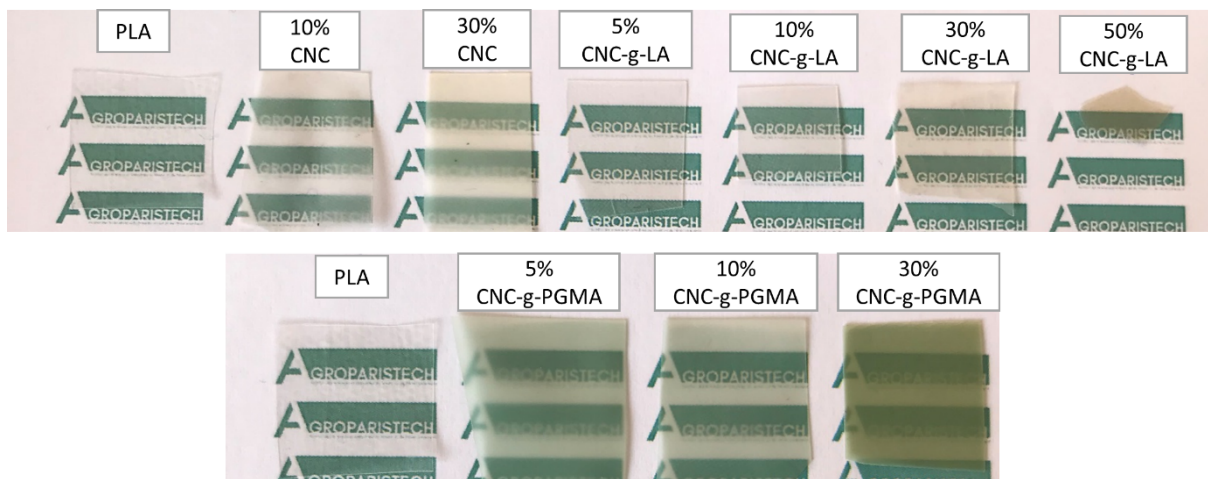


Fig. S.2. Photos of the produced PLA/CNC-g-laurci acid and PLA/CNC-g-PGMA films.

DSC scans of PLA and nanocomposites

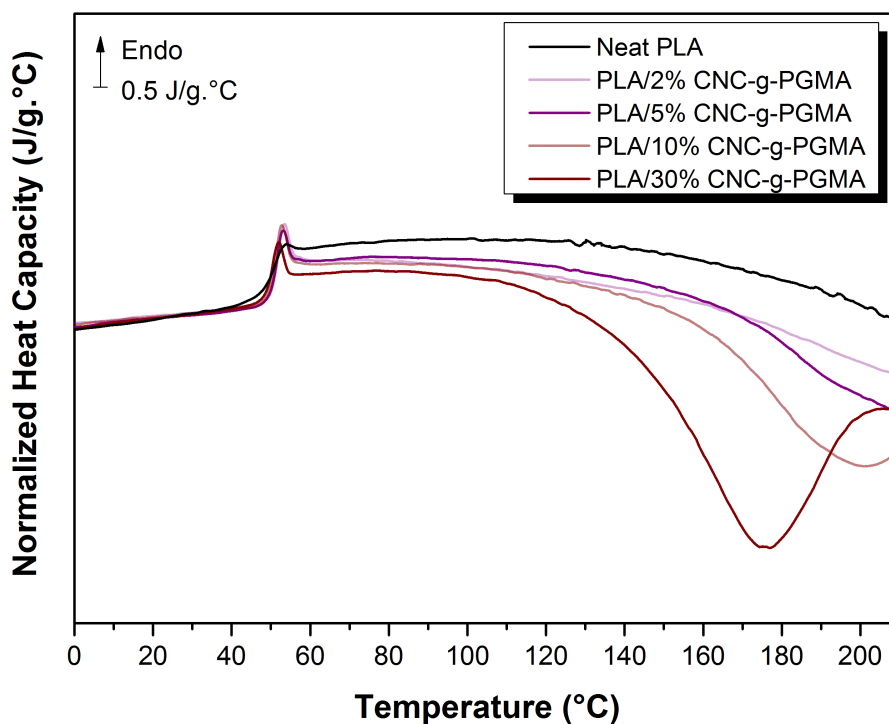


Fig. S.3. Normalized heat capacity for PLA and PLA/CNC-g-PGMA nanocomposites. It shows the glass transition of PLA at 56 °C superposed with the enthalpy of relaxation peak and a peak starting at approximately 140 °C, only observed in the first heating run. We attributed this peak to the crosslinking reaction of PGMA and PLA.

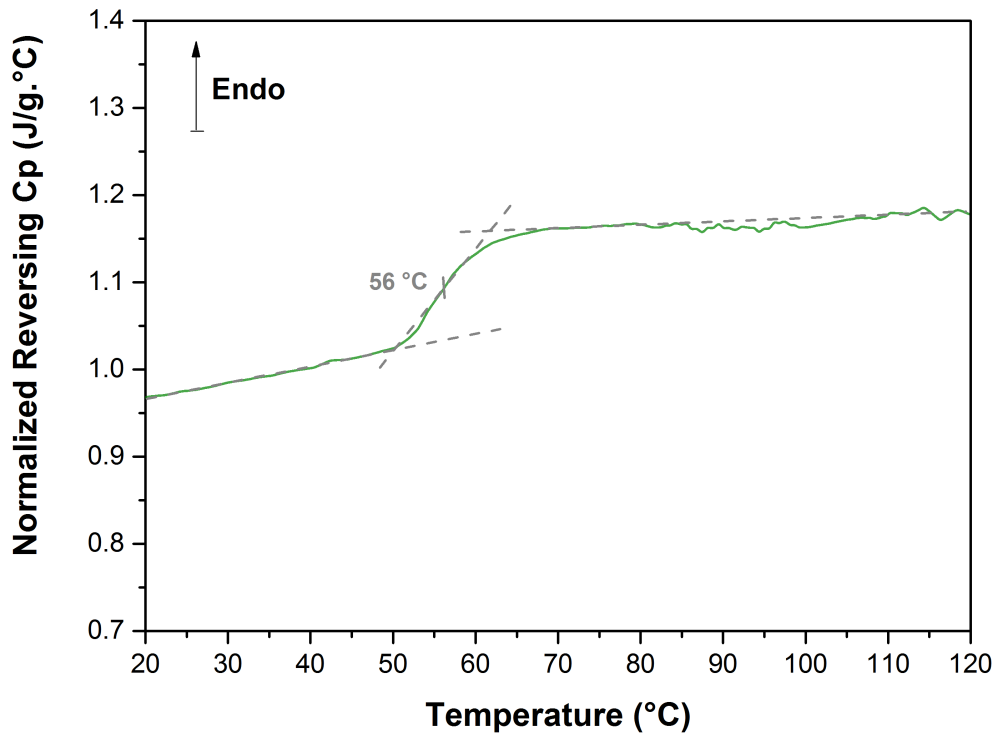


Fig. S.4. MT-DSC curve (reversing signal) of the glass transition zone for CNC-g-PGMA dry powder, measured with a heating rate of 2 °C/min.

Improvement of elastic moduli of PLA by surface grafted CNC

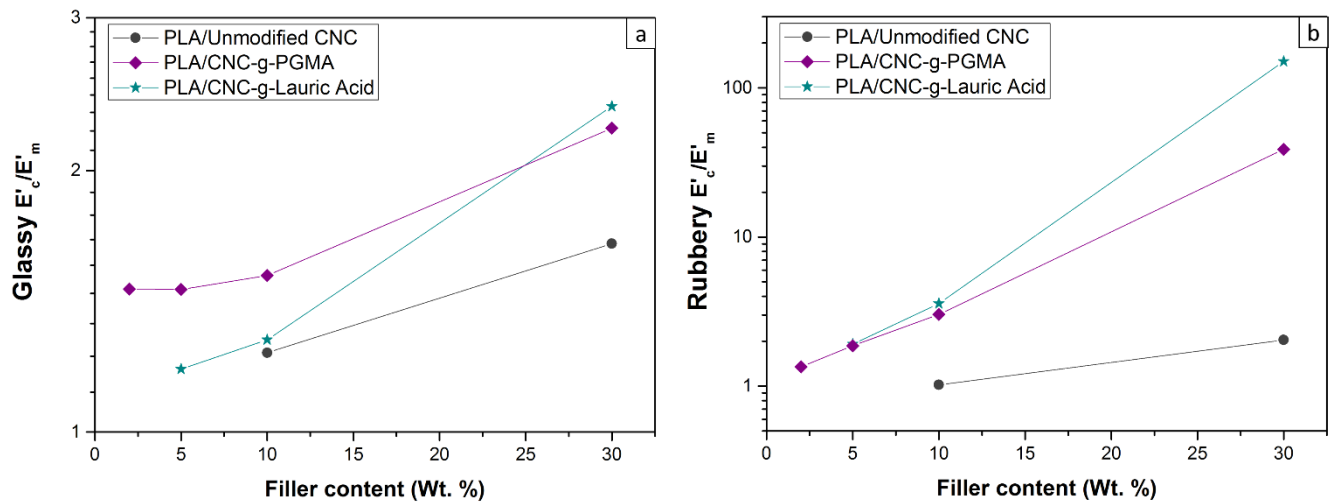


Fig. S.5. Relative glassy and rubbery storage modulus for PLA/ CNC-g-lauric acid, PLA/CNC-g-PGMA, and unmodified CNC, for contents ranging from 2 to 30 wt. %.

Halpin Tsai model: parameters screening

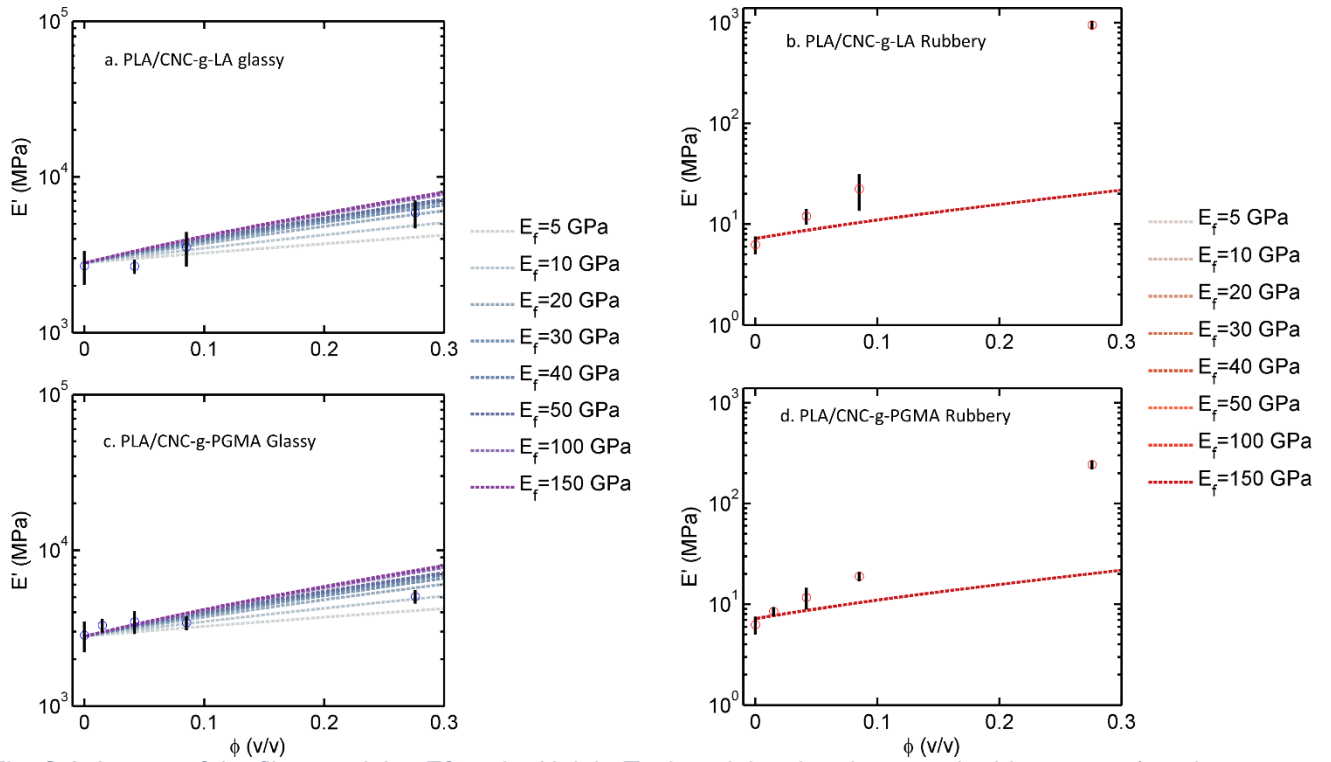


Fig. S.6. Impact of the fiber modulus E_f on the Halpin-Tsai model at the glassy and rubbery state (used aspect ratio was $\rho=11$)

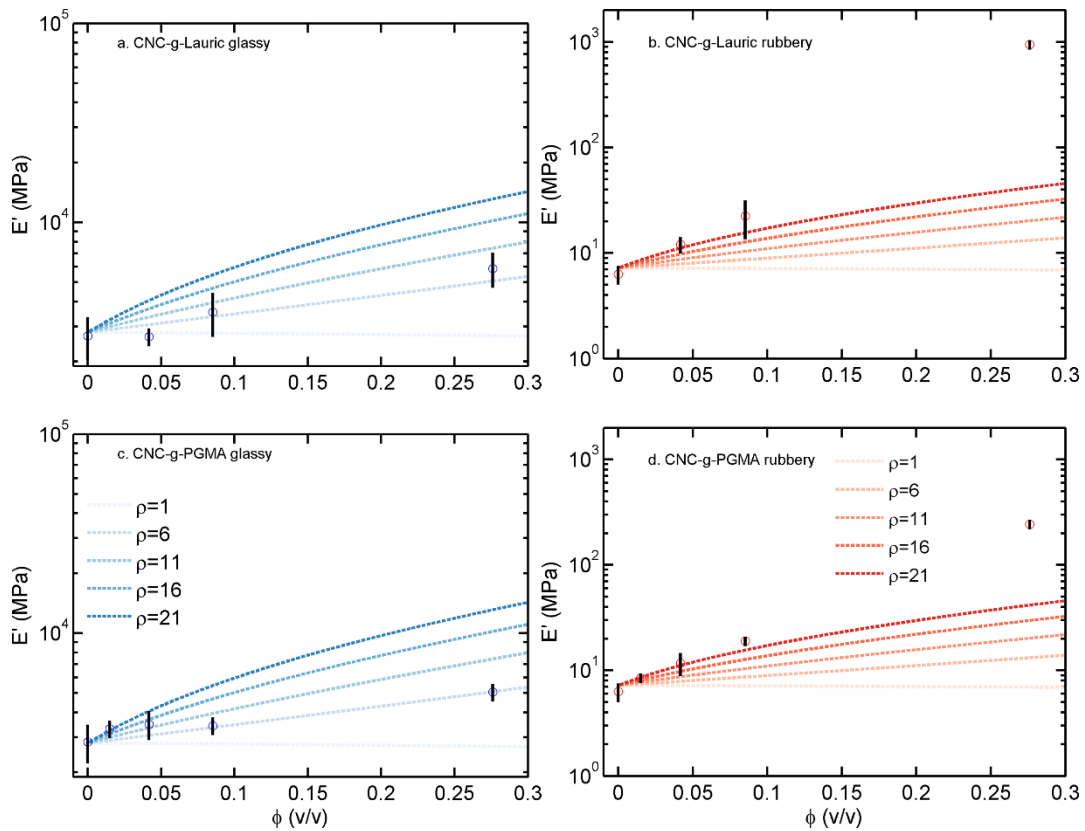


Fig. S.7. Impact of the aspect ratio ρ on the Halpin-Tsai model at the glassy and rubbery state (used fiber modulus was $E_f=150$ GPa).

Ouali percolation model: parameters screening

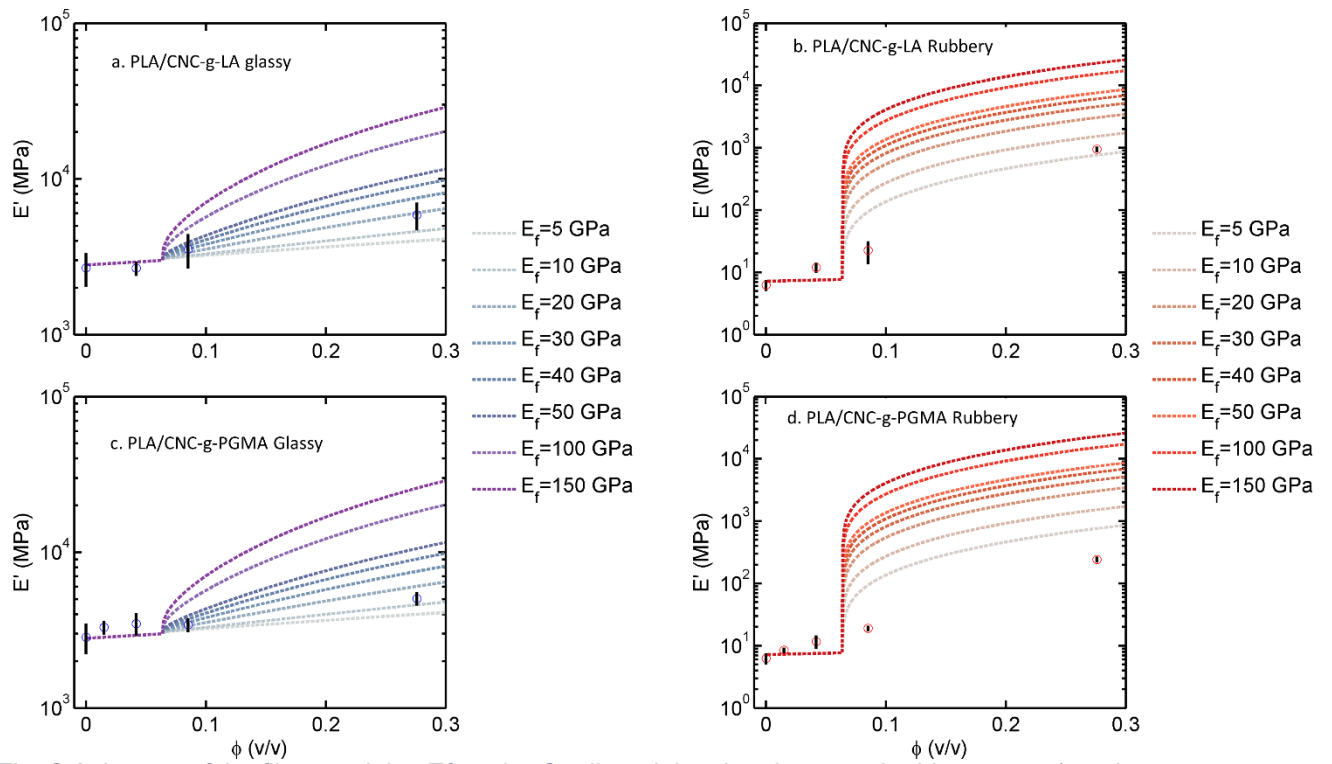


Fig. S.8. Impact of the fiber modulus E_f on the Ouali model at the glassy and rubbery state (used aspect ratio was $\rho=11$)

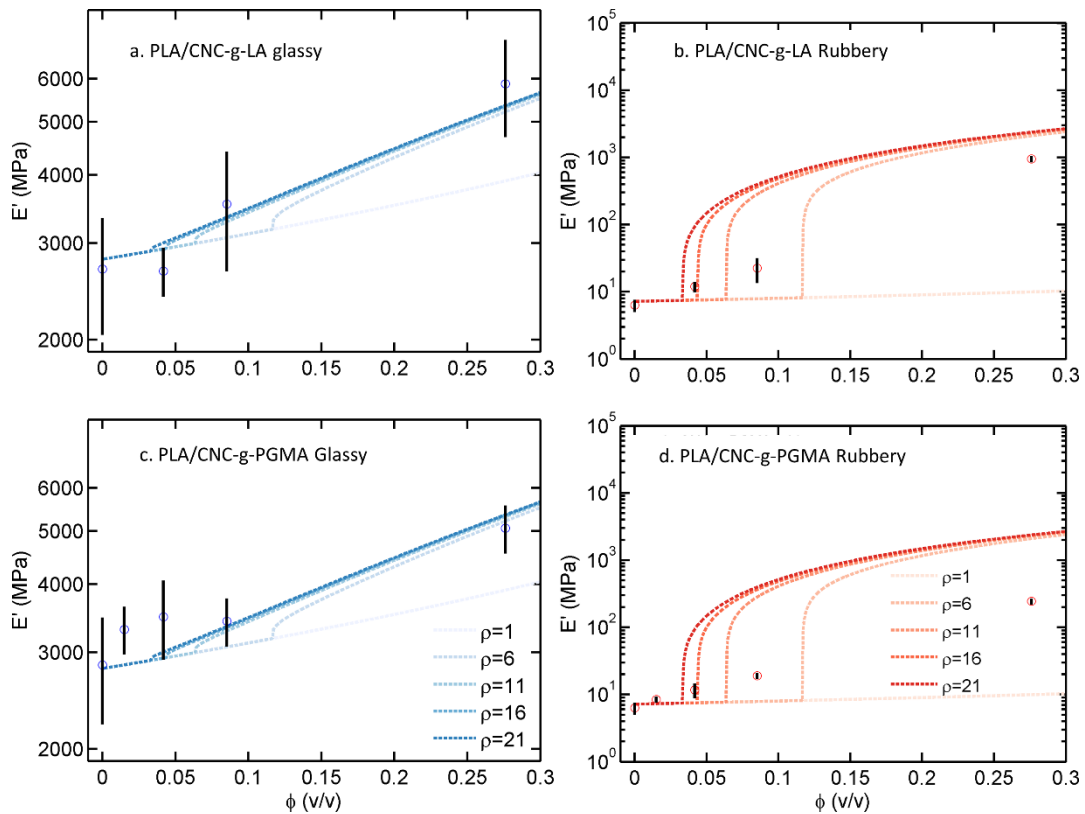


Fig. S.9. Impact of the aspect ratio ρ on the Ouali model at the glassy and rubbery state (used fiber modulus was $E_f=150$)

